Impact of riverine sediment mineralogy on seawater Nd isotope compositions in the northeastern part of the Indian Ocean during the last two glacial cycles

Yi Huang[1, 2], Christophe Colin[2*], Franck Bassinot[3], Zhaojie Yu[4], Quentin Dubois-Dauphin[2], Arnaud Dapoigny[3], David J. Wilson[5], Germain Bayon[6]

1. School of Geosciences and Info-physics, Central South University, 410083, Changsha, China.

2. Université Paris-Saclay, CNRS, GEOPS, 91405, Orsay, France.

3. Laboratoire des Sciences du Climat et de l'Environnement, LSCE/IPSL, CEA, CNRS-UVSQ, Université Paris-Saclay, F-91191 Gif-sur-Yvette, France.

4. Key Laboratory of Marine Geology and Environment, Institute of Oceanology, Chinese Academy of Science, Qingdao, China.

5. Institute of Earth and Planetary Sciences, University College London and Birkbeck, University of London, Gower Street, London, WC1E 6BT, UK.

6. Univ Brest, CNRS, Ifremer, Geo-Ocean, F-29280 Plouzané, France.

**Corresponding author: Christophe Colin – christophe.colin@universite-paris-saclay.fr*

Abstract

Radiogenic neodymium isotope compositions (εNd) are used as a tracer for water mass circulation and continental weathering at different timescales. However, uncertainties remain in the relative roles of these two factors in driving past seawater εNd variability in settings under the influence of terrestrial or riverine sediment inputs. In this study, Nd isotopes of mixed planktonic foraminifera species and $\delta^{18}O$ and $\delta^{13}C$ of *Cibicidoides wuellerstorfi* were analyzed on three cores from the northeastern Indian Ocean to better assess the impact of lithogenic inputs from Himalayan rivers and deep-water hydrological changes on the past εNd distribution in the Bay of Bengal (BoB). Our εNd data indicate relatively homogenous and radiogenic values (from -8.4 to -7.5) during glacial periods in the BoB, similar to the composition of glacial water masses of the Southern Ocean. In contrast, interglacials were characterized by more unradiogenic εNd and a pronounced north-south gradient of ~4.5 εNd units (from -12.9 to -8.5) in bottom water, similar to the present-day distribution in the BoB, pointing to a strong lithogenic control by seawater-particulate interactions. Notably, this significant decoupling of the local Nd isotope signature from the Southern Ocean composition occurred when Himalayan riverine inputs were dominated by the erosion of Indo-Gangetic plain soils during interglacial periods, whereas the preferential delivery of fresh primary mineral assemblages during glacial periods appears to have had little impact on Nd exchange with seawater. These findings provide direct evidence that the degree of seawater-particulate exchange at continental margins is governed by the mineralogy of riverine inputs, with further implications for the use of Nd isotopes as palaeoceanographic tracers.

Key words: Foraminiferal εNd, weathering, river discharge, mineralogy, Bay of Bengal.

1. Introduction

The response of continental chemical weathering to climate change is a crucial but poorly constrained component of the Earth's carbon cycle, which has major implications for understanding both past and future changes in the climate system (Raymo and Ruddiman 1992, West et al., 2005). In this context, the Himalayas have some of the highest rates of physical and chemical erosion in the world, and thus constitute a key region for establishing the relationship between climate, erosion, and chemical weathering (Sarin et al., 1989, Colin et al., 1999, Singh and France-Lanord 2002). In addition to tectonics, climate change related to the Indian summer monsoon and glacial-interglacial variability acts as a first-order factor that controls chemical weathering and erosion in Himalayan catchments over geological timescales (Colin et al., 1999, Stoll et al., 2007, Lupker et al., 2013, Wilson et al., 2015b, Joussain et al., 2016, Yu et al., 2020).

Previous studies in the BoB have shown that the dissolved seawater Nd isotope composition (expressed in epsilon units; εNd) is highly sensitive to riverine discharge and associated lithogenic inputs from Himalayan rivers (Singh et al., 2012, Yu et al., 2017a; 2017b). Hence, the application of Nd isotopes to seawater archives in the sedimentary record can enable past changes in continental chemical weathering and erosion to be reconstructed. In the BoB, there is a north-south gradient in the modern seawater rare earth element (REE) concentrations and εNd distribution extending for more than 1000 km and to a depth of more than 2500 m, which results from the input of unradiogenic lithogenic Nd (εNd ~ -16) from large Himalayan river systems (mainly the Ganges–Brahmaputra) and margin sediments mixing with the inflowing radiogenic water masses originating from the Southern Ocean (εNd ~ -8; Singh et al., 2012, Yu et al., 2017b) (Fig. 1c). These studies further demonstrate a rapid exchange of Nd between riverine particles and seawater, indicating that it is possible for the ocean to be modified by seasonal variations in freshwater and river sediment discharges, while simultaneously suggesting that benthic fluxes have a relatively minor or more regional influence in the BoB.

Past changes in this system have been explored using foraminiferal εNd records, allowing estimates of the relative contributions of unradiogenic lithogenic Nd inputs from the Himalayas and the radiogenic Southern-Sourced Water (SSW) during the late Quaternary (Burton and Vance 2000, Yu et al., 2018, Naik et al., 2019; Bang et al., 2021, Yu et al., 2022) and the Cenozoic (Gourlan et al., 2010, Song et al., 2023). For the late Quaternary, these studies highlight the complex contribution of ocean circulation (Antarctic Bottom Water, AABW; Antarctic Intermediate Water, AAIW) and Himalayan weathering inputs to the deep- and intermediate-water εNd distribution in the BoB (Yu et al. 2017b; 2022; Naik et al., 2019).

The above findings highlight the potential of Nd isotopes to evaluate monsoonal weathering inputs and their relationship to climate fluctuations. Various mechanisms of sediment-water interactions can control the reactivity of the labile fraction of the sediment exported to the ocean and its exchange with seawater (e.g., von Blanckenburg and Nägler 2001, Howe et al., 2016, Hindshaw et al., 2018, Cass et al., 2019; Larkin et al., 2021, Abbott et al., 2022). However, to date, the mineralogical fractions that can exchange Nd with seawater in the Bay of Bengal remain largely unresolved. In the Ganges-Brahmaputra (G-B) river system, changes in the relative intensity of chemical weathering and physical erosion strongly affect the major-element geochemistry and mineralogical compositions of the siliciclastic sediments that are transferred to the BoB and the Andaman Sea (Colin et al., 1999, Colin et al., 2006, Lupker et al., 2013; Joussain et al., 2016, Zhang et al., 2019, Yu et al., 2020, Song et al., 2021). Previous clay mineralogical and Sr-Nd isotope investigations have demonstrated a climate-driven shift in the locus of erosion from mountain weathering regimes to floodplain-dominated weathering regimes during periods of high Indian summer monsoon rainfall (Colin et al., 1999, Colin et al., 2006, Joussain et al., 2016, Yu et al., 2020), which provides an opportunity to explore the effect of those changing inputs on seawater Nd isotopes.

In this study, the Nd isotope composition of mixed planktonic foraminifera, combined with carbon and oxygen stable isotopes of benthic foraminifera *Cibicidoides wuellerstorfi,* were analyzed on three sediment cores located in the Andaman Sea (cores MD77-169 and MD77-171) and the BoB (core MD12-3412), spanning the last two glacial–interglacial cycles. Our aim is to reconstruct seawater εNd values for the last two climate cycles in the BoB and the Andaman Sea, and to estimate the impact of changes in lithogenic and mineralogical inputs from Himalayan rivers obtained in previous studies on the Nd isotope compositions of seawater. Overall, our new results allow us to better constrain the Nd isotope cycling in the BoB and the use of Nd isotopes for reconstructing weathering inputs from the Himalayas.

2. Materials and methods

2.1 Sediment cores

Cores MD77-169 (10°12’5 N, 95°03’0 E; 2360 m water depth) and MD77-171 (11°45’6 N, 94°09’0 E; 1760 m water depth) were collected on seamounts in the central Andaman Sea during the OSIRIS III cruise aboard the *R/V Marion Dufresne I* in 1977 (Fig. 1a). The lithologies of both cores are homogeneous, dominated by olive-grey terrigenous muddy clay and nannofossil carbonate ooze. Core MD12-3412 (17°10’94 N, 89°28’92 E; 2383 m water depth) was collected in the northern part of the BoB during the MD191/MONOPOL expedition of the French *R/V Marion Dufresne II* in 2012 (Bassinot et al., 2012). It was retrieved on the upper part of the Bengal deep-sea fan, away from the active channel system (Curray et al., 2003) (Fig. 1a). Core MD12-3412 displays a relatively continuous fine-grained hemipelagic sedimentation punctuated by episodic gravity-flow sediment layers that occurred solely during glacial periods (Joussain et al., 2016). Note that all samples used in this study were collected outside turbidite deposits to avoid any possibility of sediment reworking.

2.2. Benthic foraminifera $\delta^{18}O$ and $\delta^{13}C$ analyses

Measurements of $\delta^{18}O$ and $\delta^{13}C$ were performed on benthic foraminifera *Cibicidoides wuellerstorfi* on 149 and 190 samples from cores MD77-169 and MD12-3412, respectively. Approximately 4-8 clean and well-preserved specimens (>250 μm) were selected per sample. Analyses were carried out on a Finnigan MAT 251 mass spectrometer at the *Laboratoire des Sciences du Climat et de l'Environnement* (LSCE, France). The mean external reproducibility of carbonate standards is better than ±0.05‰ for $\delta^{18}O$ and ±0.03‰ for $\delta^{13}C$. The $\delta^{18}O$ and $\delta^{13}C$ values were calibrated versus PDB using National Bureau of Standards (NBS) standards.

2.3. Foraminiferal neodymium isotope analyses

Neodymium isotopes were measured on ~30 mg mixed planktonic foraminifera from the >150 μm size fraction, with no oxidative-reductive cleaning procedure, as this approach has been demonstrated to be suitable for extracting deep-water Nd isotope compositions (e.g., Tachikawa et al., 2014, Wu et al., 2015). Neodymium was then separated following the analytical procedure of Copard et al. (2010).

The $^{143}Nd/^{144}Nd$ ratios of purified Nd fractions were measured by Multi-Collector Inductively Coupled Plasma Mass Spectrometry (MC-ICP-MS, *Thermo Fisher Neptune^{Plus}*) at the *LSCE* (France). The solutions were analyzed at a concentration of 10 to 15 ppb. Mass bias correction was made by normalizing $^{146}Nd/^{144}Nd$ to 0.7219, applying the exponential-fractionation law. During the analysis, every group of three samples was bracketed with the JNdi-1 standard with Nd concentrations similar to those of the samples. Replicate analyses of the JNdi-1 standard yielded mean $^{143}Nd/^{144}Nd$ ratios of 0.512108 ± 0.000009 (2σ, n=32), closely matching the accepted value of 0.512115 ± 0.000006 (Tanaka et al., 2000). During the course of this study, the external reproducibility (2σ) of εNd values inferred from JNdi-1 analyses ranged between ~0.2 and 0.4 εNd units. The reported analytical uncertainty is the combination of the external reproducibility of the within-session standards and the internal measurement error of each sample. Total blanks were <30 pg and were negligible (<0.1%) in analyzed samples. Neodymium isotope compositions are expressed as $\varepsilon Nd = [(^{143}Nd/^{144}Nd)_{sample}/(^{143}Nd/^{144}Nd)_{CHUR}-1]\times10000$, with the present-day $(^{143}Nd/^{144}Nd)_{CHUR}$ of 0.512638 (Jacobsen and Wasserburg 1980).

3. Results

3.1 Benthic foraminiferal $\delta^{18}O$ and age models

The chronologies of cores MD77-169 and MD12-3412 are based on a combination of $\delta^{18}O$ stratigraphy of the benthic foraminifera *C. wuellerstorfi* and Accelerator Mass Spectrometry (AMS) ^{14}C dates obtained on samples of monospecific foraminifera (*G.ruber*, *G. trilobus,* and *G.sacculifer*) (Colin et al., 1999; Joussain et al., 2016). Cores MD77-169 and MD12-3412 display a similar range in *C. wuellerstorfi* $\delta^{18}O$ values from ~2.5 to ~4.3‰ (Fig. 2a), with a glacial to interglacial $\delta^{18}O$ difference of ~1.8‰ between enriched $\delta^{18}O$ during glacials and depleted $\delta^{18}O$ during interglacials (Fig. 2a). Smaller decreases occurred in the warm substages of marine isotope stage (MIS) 5e, 5c, and 5a for both cores. Their age models for the last 40 cal ka BP are based on 13 and 7 AMS ^{14}C dates, respectively (Colin et al., 1999 ; Joussain et al., 2016). Before 40 kyr, the benthic foraminifera *C. wuellerstorfi* $\delta^{18}O$ downcore trends of cores MD77-169 and MD12-3412 are tuned to the LR04 record using *AnalySeries* software to establish the age models (Fig. S1). These two cores provide a continuous sedimentary record extending down to MIS 8 (~290 kyr) for core MD77-169 and to MIS 6 (~182 kyr) for core MD12-3412 (Fig. 2a and Fig. S1). The accumulation rates during glacial MIS 2, 3, 4, and 6

(~7.7 to 11.7 cm/kyr for core MD77-169, and 6.8 cm/kyr for core MD12-3412) were greater than during interglacial MIS 5 (~4 cm/kyr for core MD77-169, and 3.4 cm/kyr for core MD12-3412). For core MD77-171, the age model was previously published by Yu et al. (2020) and is based on $\delta^{18}O$ stratigraphy of the planktonic foraminifera *Globigerinoides ruber.*

3.2 Benthic foraminiferal $\delta^{13}C$

The $\delta^{13}C$ values of *C. wuellerstorfi* in cores MD77-169 and MD12-3412 range from -0.69‰ to 0.46‰ and -0.67‰ to 0.51‰, respectively (Table S1, Fig 2b), with relatively high $\delta^{13}C$ values during interglacial MIS 7, MIS 5, and MIS 1, and lower values during the intervening glacials. In both cores, the $\delta^{13}C$ values also show a long-term trend, with a consistent increase of ~0.4‰ from early MIS 6 to the Holocene core top.

3.3 Neodymium isotope compositions

For core MD77-169 (central Andaman Sea), foraminiferal εNd values range from -9.8±0.1 to -7.5±0.2, with lower values during interglacial MIS 1, 5 and 7 (mean of -9.0±0.2; n=12) than during glacial MIS 2, 3, 4, and 6 (mean of -7.9±0.2; n=22) (Table S2, Fig. 2c). The deglaciations are characterized by a decrease in εNd values, but with a significant lag behind the deglacial benthic $\delta^{18}O$ decrease. Specifically, the lowest εNd values are reached ~12 kyr later than the minima in the benthic $\delta^{18}O$ record (Fig. 2a and 2c). This observation is particularly clear for Terminations I (from MIS 2 to MIS 1) and II (from MIS 6 to MIS 5), and to a lesser extent for Termination III (from MIS 8 to MIS 7).

Foraminiferal εNd values of core MD77-171 (central Andaman Sea) range from -8.7±0.1 to -6.0±0.1 (Table S2, Fig. 2c). They show similar long-term variations to those of core MD77-169, but with a small offset to more radiogenic εNd values for MIS 5, 2, and 1. As for core MD77-171, there are lower values during interglacial MIS 1 and 5 (mean of -8.4±0.2; n=7) than during glacial MIS 2, 3, 4, and 6 (mean of -7.5±0.2; n=8). A lag between the benthic foraminiferal (*C. wuellerstorfi*) $\delta^{18}O$ record (not shown) and the foraminiferal εNd record is also observed in this core during Termination I.

Core MD12-3412 (northern BoB) displays larger foraminiferal εNd variations, from -12.9±0.2 to -7.3±0.2. Interglacial εNd values (mean of -11.2±0.1; n=16) are around 3 εNd units lower than glacial εNd values (mean of -8.4±0.1; n=33) (Table S2, Fig. 2d). A lag of ~8-12 kyr between the benthic $\delta^{18}O$ and foraminiferal εNd records is also observed in this core during Terminations I and II (Fig. 2a and 2d), with foraminiferal εNd values having been analyzed at a very high temporal resolution during the latter termination.

4. Discussion

4.1 Glacial–interglacial changes in seawater Nd isotopes in the BoB: Southern-Sourced Water versus lithogenic input from Himalayan rivers

Neodymium isotope compositions of uncleaned planktonic foraminifera have been shown to record the dissolved εNd composition of bottom water and/or ambient pore water (Tachikawa et al., 2014), due to post-depositional incorporation of Nd into authigenic Fe-Mn oxyhydroxide coatings (Tachikawa et al., 2013). In the BoB, mixed planktonic foraminifera samples of late Holocene age clearly record the εNd signature of the deep-water masses and not the surface waters or the detrital sediment signatures (Yu et al., 2018). Similarly, the late Holocene core-top foraminifera sample from core MD12-3412 also displays an εNd value (-12.6±0.1; Fig. 2d) that is comparable to the modern deep-water measurements from a nearby station (Station 0810, -12.2±0.4; Singh et al., 2012).

Core-top foraminifera samples from the Andaman Sea show more radiogenic values (-

9.8±0.1 for core MD77-169 and -8.7±0.1 for core MD 77-171) than the BoB (Fig. 2c and 2d). This difference likely reflects greater contributions of Nd to the Andaman Sea from the Irrawaddy River (εNd = -12.2 to -8.3, Colin et al., 1999, Damodararao et al. 2016) than the G-B river system (εNd ~-16, Singh and France-Lanord, 2002). Furthermore, the Andaman Sea is an isolated basin, with the 1800 m sill in the Great Channel restricting the inflow of deeper water masses. In addition, the sills in the Prepares Channel and Ten Degrees Channel (<800 m depth) isolate this basin from the unradiogenic εNd values in the intermediate water masses of the northern BoB (Fig. 1a; mean εNd of -14.8±0.2 at 500-1500 m water depth in the northern BoB; Singh et al., 2012). Cores MD77-169 (2360 m water depth) and MD77-171 (1760 m water depth) were collected to the north of the deepest sill of the Great Channel (1800 m) (Fig. 1a). Unfortunately, modern εNd values of deep waters in the Andaman Sea are not available. However, seawater εNd values at 1800-2500 m depth at the latitude of the Great Channel (5°N) in the BoB range from -10.5±0.2 to -9.9±0.2 (Station 0806, 5.813°N, 86.997°E, Singh et al., 2012; Station MONO1, 8°N, 89.4°E, Yu et al., 2017). Such a seawater εNd range is close to the foraminiferal εNd values obtained from the core top of MD77-169 (-9.8±0.1) (Fig. 2c), which suggests that the advection of such inflowing waters could be an important contributor of Nd to the central Andaman Sea. The slightly more radiogenic εNd values in the core top from MD77-171 (-8.7±0.1) than in those upstream waters may indicate local lithogenic inputs of radiogenic Nd, such as from Barren Island, which is a volcanic island in the Andaman-Nicobar arc (εNd ~-5 for clay-sized fraction; Ali et al., 2015), or other igneous rocks from that arc.

The benthic flux from early diagenesis of sediments has recently been proposed to strongly impact deep water Nd isotopes in some oceanic regions (Abbott et al., 2015; 2022; Haley et al., 2017). However, foraminiferal εNd values from core tops in the BoB and the Andaman Sea, in both this study and previous ones (Yu et al., 2018, Naik et al., 2019, Bang et al., 2021), are similar to the local deep water Nd isotope signatures, showing large offsets to the accompanying detrital εNd values. These observations suggest that a benthic flux does not strongly modify the Nd isotope composition of foraminifera from our studied sites in the present day. This finding is in line with the vertical distribution of dissolved REE concentrations and εNd values obtained towards the bottom of six hydrological stations collected along a north-south transect at ~89°E in the Bay of Bengal, which do not show any clear influence of benthic flux on bottom water (Yu et al., 2017a; 2017b). To the extent that this scenario has also remained the case in this region in the past, the foraminiferal records can therefore be used to establish past seawater εNd compositions.

The εNd records of our studied cores show pronounced glacial-interglacial variability during the last two climatic cycles (last ~300 kyr) (Fig. 3a), with more unradiogenic εNd values during interglacial than glacial periods. Such variations have previously been reported in Nd isotope records obtained on both mixed planktonic foraminifera and bulk sediment leachates in the northern BoB (core RC12-343, 2666 m water depth, Stoll et al., 2007) and equatorial Indian Ocean (core SK129-CR2, 3800 m water depth, Wilson et al., 2015a; ODP Site 758, 2925 m water depth, Burton and Vance 2000, Gourlan et al., 2010) (Fig. 3a), as well as in a record from the Cape Basin near the modern boundary between North Atlantic Deep Water (NADW) and Upper Circumpolar Deep Water (UCDW) (ODP 1088, 2080 m water depth, Hu et al., 2016). Those glacial-interglacial shifts in the Indian Ocean εNd composition have been interpreted as reflecting either changes in the composition of water masses advected from the Southern Ocean and/or changes in the lithogenic Nd inputs induced by an intensification of weathering during warm and humid periods (Colin et al., 1999; 2006, Burton and Vance, 2000; Gourlan et al., 2010, Piotrowski et al., 2009, Wilson et al., 2015a; Joussain et al., 2016; Naik et al., 2019; Bang et al., 2021; Yu et al., 2020).

In the studied cores MD12-3412 and MD77-169, glacial periods (MIS 2, 3, 4, 6, and 8) are characterized by relatively radiogenic values ranging from -9.4±0.1 to -7.3±0.1 (mean of -8.4±0.7; 2σ, n=33) and from -8.3±0.1 to -7.6±0.2 (mean of -7.9±0.7; 2σ, n=22), respectively (Fig. 3a). These values are comparable to glacial εNd values in equatorial Indian Ocean core SK129-CR2 (-8.5±0.4 to -6.6±0.4, Wilson et al., 2015a), ODP Site 758 on Ninetyeast Ridge (-8.6±0.1 to -7.4±0.2, Gourlan et al., 2010), and northern Indian Ocean core RC12-343 (-8.5±0.1 to -7.0±0.1, Stoll et al., 2007) (Figs. 3a and 4). Taken together, these observations indicate that the glacial bottom-water εNd compositions in the BoB and Andaman Sea were relatively homogenous and similar to the glacial εNd values of deep waters from the equatorial Indian Ocean, hence showing no significant latitudinal εNd gradient (Fig. 4). This finding hence suggests that Nd exchange associated with particle-dissolved exchange process was probably limited during glacial periods.

In the absence of any significant influence of lithogenic Nd supplied from the G-B and/or Irrawaddy rivers during glacial periods, the bottom-water εNd composition of the BoB and the Andaman Sea most likely reflected continuous ventilation by modified Circumpolar Deep Water (CDW) from the Southern Ocean. The radiogenic values likely indicate a stronger penetration of more radiogenic AABW (εNd -6.0 to -6.8 in the Antarctic; Howe et al., 2016) into the deep northern Indian Ocean and/or a reduced NADW component in the Southern Ocean during this period compared to interglacials (Piotrowski et al., 2009, Gourlan et al., 2010, Wilson et al., 2015a, Bang et al., 2021). Changes in the end-members of these water masses also dominate the distributions of εNd in other ocean basins, confirming the important role of the Southern Ocean in regulating the mixing of water masses within the global ocean circulation system (Zhao et al., 2019; Struve et al., 2019). Such a glacial reduction in nutrient-depleted North-Atlantic sourced waters in the north Indian Ocean is also supported by benthic radiocarbon evidence (Bharti et al., 2022), and is consistent with lower benthic $\delta^{13}C$ values in cores MD77-169 and MD12-3412 (Fig. 3b). The glacial $\delta^{13}C$ values in those cores are identical to those of core SK129-CR2 (3800 m) in the equatorial Indian Ocean (Fig. 3b), which suggests similar SSW sources for cores MD77-169, MD12-3412, and SK129-CR2, and a greater proportion of southern-sourced poorly-ventilated AABW inflow relative to NADW.

In contrast, the interglacial periods (MIS 1, 5, and 7) are characterized by less radiogenic εNd values in all the studied cores compared to glacials (Fig. 3a). The average εNd values during the Holocene and MIS 5 in core MD12-3412 (-12.6±0.1 and -11.2±0.6) were ~1.5 εNd units more negative than in core RC12-343 (-11.1±0.3 and -9.8±0.2; Stoll et al., 2007), and 2 to 3 εNd units more negative than in cores SK129-CR2 (-9.7± 0.8 and -9.1±0.7; Wilson et al., 2015) and ODP Site 758 (-9.7±0.7 and -9.2±0.7; Gourlan et al., 2010) from the equatorial Indian Ocean. For the Andaman Sea, core MD77-169 (-9.5±0.3 and -8.6±0.3) also had less radiogenic εNd values during interglacial than glacial periods, with similar ranges to core SK129-CR2 and ODP Site 758. In contrast to glacial MIS, seawater εNd values during the interglacials MIS 1 and 5 display large spatial variations, with a marked north-south gradient indicating an approximately linear relationship with the distance from the G-B river mouth (Fig. 4).

Past Southern Ocean εNd values were around 2.4 εNd units more radiogenic during the Last Glacial Maximum (26-19 ka, -7.8) than during the Holocene (11-0 ka, -10.2) at depths between 1300 and 3500 m (Hu et al., 2016), similar to the glacial-interglacial shift in the southern BoB at 5°N (ODP Site 758) (Fig. 3a). However, changes in the Southern Ocean cannot explain the north-south gradient observed in the BoB during MIS 1 and 5, when unradiogenic εNd values in the northern BoB reached as low as -12.9 in core MD12-3412, ~500 km from the G-B river mouth (Fig. 4). This εNd gradient is comparable to modern seawater gradients in the BoB (Singh et al., 2012; Yu et al., 2017b) (Fig. 4), with seasonal variations in those gradients attributed to seasonal changes in freshwater and sediment discharge from the G-B river system induced by the Indian monsoon (Yu et al., 2017b In the modern BoB, the spatial seawater εNd distribution results mainly from the release of Nd from detrital sediments, which can modify seawater εNd values to depths >2500 m in the water column (Fig. 1c). Evidence for pronounced seasonal changes in εNd values in the modern BoB suggests that such Nd exchange is rapid and mainly occurs within the water column (Yu et al., 2017b). Thus, the large north-south gradient of seawater εNd values reconstructed during MIS 1 and 5 appears likely to have been related to strong modification by lithogenic Nd inputs from detrital sediments supplied by the G-B river system (Fig. 4). Because it is closer to the mouth of the G-B river system than core SK129-CR2 and ODP Site 758, the water column above core MD12-3412 receives a greater input of detrital sediments, which leads to a greater overprinting of local seawater with unradiogenic εNd values during interglacials (Fig. 3a).

The benthic $\delta^{13}C$ values are higher during interglacials compared to glacials in cores MD77-169 and MD12-3412, except for a long-term increasing trend since MIS 5, which could be attributed to changes in the global carbon cycle (Wang et al., 2004, Hoogakker et al., 2006; Wilson et al., 2015a) (Fig. 3b). The interglacial $\delta^{13}C$ values for those cores are generally similar to those of core SK129-CR2 (Fig. 3b), and likely reflect a higher contribution of NADW to the Southern Ocean (Piotrowski et al., 2008) and its northwards penetration into the northern Indian Ocean (Wilson et al., 2015a). However, the $\delta^{13}C$ values during MIS 5 are slightly lower in cores

MD77-169 and MD12-3412 compared to core SK129-CR2, and are temporally variable in all three cores. Since benthic $\delta^{13}C$ values can also be influenced by changes in biological productivity and nutrient regeneration (e.g., Piotrowski et al., 2009; Wilson et al., 2015a), the lower values in the northern BoB and the Andaman Sea might also reflect enhanced regional productivity and/or increased terrigenous organic carbon inputs with low $\delta^{13}C$ values.

4.2 Impact of fluxes and mineralogy of detrital terrigenous inputs from Himalayan rivers on seawater εNd values

For core MD77-169, located in the central Andaman Sea, the εNd values of detrital sediments display a narrow range from -11 to -9.5 (Fig. 5a) (Colin et al., 2006), suggesting that detrital material at this site was derived mainly from the Irrawaddy River (εNd ~ -12.2 to -8.3) during the last two glacial-interglacial cycles (Colin et al., 1999, 2006). For core MD12-3412, located in the northern Bay of Bengal, the εNd values of detrital sediments range from -13.3 to -9.7 (Fig. 5b) (Joussain et al., 2016), indicating mixing between sediments from the G-B river system (εNd ~ -16) and from rivers draining the western part of the Indo-Burman Ranges (εNd from +0.3 to -8) and the Irrawaddy River (εNd from -8.3 to -12.3) (Colin et al., 1999; Joussain et al., 2016; Damodararao et al., 2016). The more unradiogenic detrital εNd values in core MD12-3412 during interglacials (Fig. 5b) imply higher relative contributions of detrital sediments from the G-B river system (Joussain et al., 2016). Overall, the εNd values of the carbonate-free detrital sediments from both cores are generally more unradiogenic than the foraminiferal εNd values, with the values for the latter during interglacial periods being in the range of measured or expected modern seawater dissolved εNd values at the core locations. Hence, glacial-interglacial variations in the detrital εNd values in cores MD77-169 and MD12-

3412 fail to explain the observed variability of past seawater εNd compositions reconstructed for the northern BoB and Andaman Sea (Fig. 5). For core MD77-169, this finding is particularly clear, since the detrital fractions do not display any significant glacial–interglacial εNd fluctuations (Fig. 5a). For core MD12-3412, the foraminiferal εNd values from interglacial MIS 1 and 5 are relatively similar to the corresponding detrital fractions, albeit slightly more radiogenic. In contrast, the εNd offset between the two fractions is far greater (up to 2 εNd units) during glacial periods (MIS 2, 3, 4 and 6; Fig. 5b). On this basis, we conclude that past changes in the bottom-water εNd composition of the BoB cannot be directly linked to a change in sediment provenance across the Himalayan catchments.

It has been demonstrated that terrigenous fluxes to the northern BoB were systematically higher during glacial periods (>10 $g.cm^{-2}.kyr^{-1}$) than during interglacial periods (<5 $g.cm^{-2}.kyr^{-1}$) (Colin et al., 2006) (Fig. 5d). Such changes can be attributed to (i) higher physical erosion rates in the Himalayan highlands due to enhanced glacial erosion (Colin et al., 2006), and (ii) more efficient sediment transport to the deep sea due to the reactivation of submarine canyons during sea-level low stands and the resulting turbidite deposition (Joussain et al., 2016). In any case, a striking feature of our results is that the resulting increase in detrital fluxes during glacial MIS 2, 3, 4 and 6 was not accompanied by a stronger modification of seawater εNd values in the northern BoB, whereas more unradiogenic seawater εNd values prevailed during interglacials when the detrital fluxes transported to the northern BoB were lower (Fig. 5). We thus hypothesize that past changes in seawater εNd values in the BoB and the Andaman Sea were not directly controlled by variations in the terrigenous fluxes transported to the northern BoB, at least for the last climatic cycle.

Instead, we suggest that the pronounced shift towards unradiogenic seawater εNd values during interglacial intervals may have been caused by a change in the mineralogical composition of the sediment load transported to the northern BoB. Specifically, interglacial MIS 1 and 5 were both generally associated with higher (smectite+kaolinite)/(illite+chlorite) ratios in core MD12-3412 (Fig. 5c). In the BoB, illite and chlorite are likely to mainly result from the physical erosion of igneous rocks or of ancient sedimentary rocks associated with limited chemical weathering, hence being mainly sourced from upstream high-elevation catchment regions, as demonstrated for the Ganges River (Sarin et al., 1989, Huyghe et al., 2011). In contrast, smectite and kaolinite show higher concentrations in suspended particulate loads from the Indo-Gangetic floodplain (Sarin et al., 1989; Huyghe et al., 2011). This increase in the proportion of smectite in the lowlands of the river basin results either from the recycling of smectite-rich sedimentary rocks of the Siwalik Group (Sarin et al., 1989) and/or from in-situ chemical weathering during pedogenesis in the Ganges River plain (Chamley and Chamley 1989, Huyghe et al., 2011). The clay mineral composition of the Indo-Burman ranges is not yet available but, considering the lithology and the morphology of these ranges, we assume that their erosion would mainly deliver illite and chlorite, with a negligible amount of smectite and kaolinite. Hence, the (smectite+kaolinite)/(illite+chlorite) ratio is likely to be largely independent of the relative contributions of the different sedimentary sources (G-B river system versus rivers of the Indo-Burman ranges), and can be used (to a first approximation) as an index to trace chemically-weathered inputs derived from floodplains versus primary mineral assemblages associated with physical erosion in high-relief regions of the river basins (Colin et al., 2006; Joussain et al., 2016; Yu et al., 2020).

The (smectite+kaolinite)/(illite+chlorite) ratios in all cores from the northern BoB (including core MD12-3412) indicate a higher input of detrital material from the highlands of the river basins (illite and chlorite) during glacial MIS 2, 3, 4, and 6 than during interglacial MIS 1 and 5 (Fig. 5c). In contrast, the interglacials MIS 1 and MIS 5 (especially the warm substages of MIS 5) were characterized by higher smectite and kaolinite contents. These interglacial (smectite+kaolinite)/(illite+chlorite) maxima (Fig. 5c) were temporally associated with an intensification of summer monsoon rainfall (Joussain et al., 2016; Yu et al., 2020; Wang et al., 2022) (Fig. 5e), which would have led to higher physical erosion and chemical weathering rates in the Indo-Gangetic floodplain, thus both inducing smectite formation and increasing its transfer to the BoB.

The above results indicate that seawater-particulate interactions (resuspension of sediments by strong deep currents and/or particulate-seawater interactions within the water column) in the BoB and the associated shifts in seawater Nd isotope composition strengthened at times when the suspended sediment load delivered by Himalayan rivers to the northern BoB was dominated by smectite-kaolinite clay mineral assemblages from the Indo-Gangetic floodplains (Fig. 5). Such a hypothesis of a greater reactivity of mature clay mineral assemblages in seawater is consistent with inferences from the northern South China Sea that marine sediments enriched in pedogenic clays from Chinese tropical soils (dominated by kaolinite, smectite, and other pedogenic minerals such as iron oxides) are more efficient in exchanging Nd with seawater than marine sediments derived from physical erosion in the uplands of Taiwan (enriched in illite, chlorite, and fresh primary minerals) (Huang et al., 2023). While enhanced physical erosion in glaciated continental areas can also influence the Nd isotope composition of seawater (Zhao et al., 2019), the preferential dissolution of smectite has been shown to control the Nd budget of pore waters offshore of the Antarctic Peninsula shelf (Wang et al., 2022). Additionally, the preferential dissolution in the marine environment of kaolinite exported from tropical regions can also act as a net source of light REE to seawater (Bayon et al., 2023), and hence could represent a possible mechanism explaining the pronounced εNd shift towards unradiogenic compositions during interglacial periods in the BoB.

Therefore, we argue that the enhanced delivery of smectite-kaolinite or other pedogenic minerals such as iron oxides during periods of high-intensity chemical weathering during interglacial periods is more likely to influence the seawater Nd isotope composition in comparison to periods dominated by inputs of primary mineral assemblages. As such, these changes could be driven by Indian summer monsoon rainfall changes in response to both local orbital forcing and global glacial–interglacial changes (Fig. 5e, Wang et al., 2022). While future studies would be required to further investigate the clay mineral phases controlling seawater-particulate Nd exchange in the BoB, as well as the potential influence of pedogenic iron oxide phases (Larkin et al., 2021), our results indicate that the shift towards unradiogenic seawater εNd values and pronounced latitudinal gradients in the northern BoB during interglacial periods is likely to result from enhanced inputs of pedogenic minerals.

4.3 Role of Southern-Sourced Water and Indonesian Throughflow intensity in driving seawater εNd values

During glacial–interglacial transitions, foraminiferal εNd variations in the northern BoB (MD12-3412) and the northern Andaman Sea (MD77-169) appear to have lagged behind changes in the benthic $\delta^{18}O$ records (Fig. 6a and 6b). In both settings, the εNd values shifted later than $\delta^{18}O$ values during Terminations I (offset of ~8 kyr) and II (offset of up to ~12 kyr) (Fig. 6a and 6b). The longer record from core MD77-169 also suggests a similar offset during

Termination III (~8 kyr) (Fig. 2a and 2b). These observations agree with previous studies reporting similar offsets for intermediate- and deep-water εNd records in the BoB during Termination I (Yu et al., 2018, 2022).

During Termination II, the decrease in the benthic $\delta^{18}O$ record occurred in phase with the increase in the (smectite+kaolinite)/(illite+chlorite) ratio in core MD12-3412 (Fig. 5c). Such variations coincided with stronger Northern Hemisphere insolation and enhanced Indian summer monsoon rainfall over the G-B river basin (Joussain et al., 2016; Yu et al., 2020; Wang et al., 2022) (Fig. 5e). Hence, while there is strong evidence for increased rainfall and higher lithogenic input from the Indo-Gangetic floodplains during the warm substage of MIS 5e, the seawater εNd composition remained relatively radiogenic and the unradiogenic peak occurred several thousand years after the peak of MIS 5e (Fig. 6b). In agreement with recent work (Yu et al., 2018, 2022), these findings suggest that the greater inputs of unradiogenic lithogenic material from the Himalayan rivers during glacial-interglacial transitions and the early Holocene and Eemian climate optima were partially buffered by persistent strong northward penetration of radiogenic SSW and/or additional inputs of radiogenic Nd.

Records at intermediate depths have shown that stronger ventilation of SSW (AAIW) contributed to the northern Indian Ocean during Termination I and into the early Holocene, resulting in radiogenic seawater εNd values, even though the BoB received increased riverine discharge (Yu et al., 2018, Ma et al., 2020, Yu et al., 2022). Consequently, it is possible to hypothesize that cores MD77-169 and MD12-3412 at deeper depths might also have been strongly influenced by SSW with radiogenic Nd isotope compositions during Terminations I and II.

During Termination I, inputs of freshwater may have played a role in the reduced formation and shoaling of NADW (Elliot et al., 2002) and a decreased export of NADW into the South Atlantic (Freeman et al., 2015), the Pacific Ocean (Galbraith et al., 2007), and the Indian Ocean (Piotrowski et al., 2009, Ahmad et al., 2012, Nisha et al., 2023). This scenario would imply a greater contribution of $\delta^{13}C$-depleted SSW (AABW or CDW) into the northern Indian Ocean during this period, which is supported by decreases in benthic $\delta^{13}C$ values from 18-14.7 kyr BP (Heinrich Stadial 1) and 12-10.5 kyr BP in cores MD77-169 and MD12-3412 (Fig. 6d). During Termination II, there was a similar drop in $\delta^{13}C$ values during the interval of the lagging εNd record in early MIS 5e (Fig. 6d). Hence, reduced NADW production and export could similarly account for the decoupling between the εNd record and the $\delta^{18}O$ record at this time.

Nevertheless, the deglacial and early interglacial decoupling between seawater εNd values and benthic $\delta^{18}O$ values is not observed at deeper depths in the equatorial Indian Ocean (core SK129-CR2, 3800 m) (Fig. 6c). Due to the topography of the Ninetyeast Ridge (Fig. 1a), core SK129-CR2 lies on a different pathway of the SSW inflow compared to some of the upstream inflow to the cores in the northern BoB and the Andaman Sea. Cores MD77-169 and MD12-3412 are located on the pathway of SSW flowing along the margin of Western Australia and the volcanic arc of Java-Sumatra before it enters the BoB and the Andaman Sea (via the Great Channel) (Fig. 1a). This observation indicates possible intra-basin differences in the Nd isotope composition of the SSW during glacial–interglacial cycles (Lathika et al., 2021). Modern intermediate-water and deep-water masses flowing northwards via the eastern route to the eastern equatorial Indian Ocean are strongly modified by vertical mixing with radiogenic western Pacific waters (εNd ~-4.1 to -4.8) which enter the Indian Ocean via the Indonesian Throughflow (ITF). In the eastern equatorial Indian Ocean, intermediate-deep waters (unfiltered) display radiogenic εNd values (-5.3 to -3.8) to a depth of more than 1500 m due to the pronounced mixing with the radiogenic waters of the ITF (Jeandel et al., 1998). On this basis, we therefore hypothesize that the intensification of the ITF during glacial–interglacial sea-level rise (Pang et al., 2021; Le Houedec et al., 2024) induced more radiogenic values in the intermediate and deep-water masses flowing into the BoB and Andaman Sea during deglacial and early interglacial periods.

In Figure 7, we compare a proxy record of the ITF intensity from Pang et al. (2021) to the calculated seawater Nd isotope gradient (ΔεNd) between the records from core MD12-3412 in the northern BoB and core SK129-CR2 in the equatorial Indian Ocean. The ΔεNd record represents the north-south gradient of the BoB through time, with the unradiogenic values during interglacials largely reflecting the inputs from the G-B river system. The abnormal radiogenic ΔεNd values during MIS 5e and the early Holocene were associated with an intensification of the ITF (Fig. 7c). In addition, intensification of the Indian monsoon rainfall during the early Holocene and MIS 5e (Zorzi et al., 2015) could also have been associated with greater rainfall and weathering of the volcanic rocks in the Indonesian archipelago (e.g. Java, Sumatra, Sulawesi) where the ITF circulates. Such enhanced weathering of this volcanic province could have further modified the Nd isotope composition of intermediate-water and deep-water masses reaching the BoB and the Andaman Sea via the eastern Indian Ocean, producing a more radiogenic signature. Further investigation of sediment cores proximal to the margins of Java and Sumatra will be necessary to constrain the extent to which the intermediate-water and deep-water masses of the BoB are influenced by such upstream mechanisms.

While adding some complexity to the interpretation of our seawater εNd records, the above-mentioned observations of a significant decoupling between seawater εNd and benthic $\delta^{18}O$ records during glacial-interglacial transitions have no effect whatever on the validity of the main conclusion of this study.

5. Conclusions

Neodymium isotope compositions of planktonic foraminifera, combined with oxygen and carbon isotopes of benthic foraminifera *C. wuellestorfi,* were analyzed on sediment cores from the Andaman Sea and the Bay of Bengal (BoB) spanning the last two glacial-interglacial cycles. Our aim was to reconstruct past seawater εNd changes and to constrain the impact of changes in lithogenic sediment flux and mineralogy on the εNd distribution in the BoB and Andaman Sea.

During glacial periods, all records from the BoB displayed more radiogenic seawater εNd values (-8.4 ~ -7.5) than today and there was greatly reduced spatial variability, consistent with a dominant control from the intrusion of radiogenic SSW. Although glacial periods were associated with enhanced lithogenic fluxes and intense physical erosion of the highlands of the Himalayan River basins, they were not associated with less radiogenic εNd values in the core (MD12-3412) located in close proximity to the river mouth. In contrast, interglacial MIS 1 and 5 were characterized by less radiogenic εNd values in core MD12-3412 (mean of -11.2) and a pronounced north-south gradient of up to 3 εNd units in the BoB, similar to the modern seawater distribution. Those more unradiogenic εNd values coincided with higher (smectite+kaolinite)/(illite+chlorite) ratios in the sediments of the northern BoB, reflecting enhanced sedimentary inputs of weathered material from the Indo-Gangetic plain soils.

This finding illustrates that river sediment discharges dominated by smectite-kaolinite mineral assemblages are more likely to exchange Nd with seawater in the northern BoB than those carrying primary minerals produced by physical erosion in the Himalayan highlands. It emphasizes the need to take sediment mineralogy of riverine input into considerations in application of εNd as a proxy to reconstruct modern and past hydrology.

List of figures:

Fig. 1. (a) Geographical setting and locations of sampled cores (red circles) and reference sites (dark blue circles) in the Bay of Bengal (BoB) and Andaman Sea. The arrows illustrate the general surface (black) and deep (blue) circulation patterns in the BoB during boreal summer (June–September) (Varkey et al., 1996; Shankar et al., 2002). The values represent the εNd values of riverine detrital sediment(Colin et al., 1999; Singh et al., 2008). Chart pies represent the clay assemblage of different rivers surrounding the Bay of Bengal (Huyghe et al., 2011). (b) Salinity distribution along a north-south cross-section at 89°E in the BoB (white dashed line). The salinity data are from the World Ocean Atlas 2013 (Zweng et al., 2013). EIOW: Eastern Indian Ocean Surface Water; ASHS: Arabian Sea High Salinity Water; BoBLS: BoB Low Salinity Water; BoBIW: BoB Intermediate Water; NIIW, North Indian Intermediate Water; NIDW: North Indian Deep Water; AABW: Antarctic Bottom Water. Surface, intermediate, and deep-water mass hydrology shown in Figure 1 are discussed in detail in the Supplementary Information (regional setting). (c) Dissolved seawater εNd distribution along a north-south cross-section at 87°E in the BoB (black dashed line, Singh et al., 2012).

Fig. 2. (a) $\delta^{18}O$ and (b) $\delta^{13}C$ records from benthic foraminifera *C. wuellerstorfi* in cores MD77-169 and MD12-3412. (c) εNd values of mixed planktonic foraminifera in cores MD77-169 and MD77-171. (d) εNd values of mixed planktonic foraminifera in core MD12-3412. Marine isotope stage (MIS) numbers are labelled along the top and glacial periods are shaded in blue

(in this figure and subsequent figures). The glacial terminations are indicated by the grey rectangles.

Fig 3. (a) Foraminiferal εNd records, (b) $\delta^{13}C$ and (c) $\delta^{18}O$ records of benthic foraminifera *C. wuellerstorfi* in core MD77-169 (this study), core MD12-3412 (this study), core RC12-343 (Stoll et al., 2007; εNd record only), ODP Site 758 (Chen et al., 1995), and core SK129-CR2 (Wilson et al., 2015a).

Fig 4. εNd values versus latitude in the BoB. Comparison of planktonic foraminiferal εNd values from interglacial (Holocene and MIS 5) and glacial periods (Stoll et al., 2007; Gourlan et al., 2010, Wilson et al., 2015a; this study) with modern dissolved εNd values in the deep-water masses of the BoB (Singh et al., 2018; Yu et al., 2018). The composition of modern and glacial Circumpolar Deep Water (CDW) and Ganges-Brahmaputra riverine inputs is also shown (see text).

Fig. 5. (a, b) εNd values of the carbonate-free detrital fraction and mixed planktonic foraminifera in cores MD77-169 (a, Colin et al., 2006; this study) and MD12-3412 (b, Joussain et al., 2016; this study). (c) Ratio of (smectite+kaolinite)/(illite+chlorite) in core MD12-3412 (Joussain et al., 2016). (d) Detrital flux ($g.cm^{-2}.kyr^{-1}$) in nearby cores MD77-180, MD77-181, and MD77-183 from the northern BoB (Colin et al., 2006). (e) Ice volume–corrected δD based on the average of four homologs (n-C27, n-C29, n-C31, and n-C33) from sediment core SO17286-1 in the BoB as a proxy for rainfall amount (Wang et al., 2022). The dashed black curve is the summer (July) insolation at 10°N.

Fig. 6. (a) $\delta^{18}O$ and (d) $\delta^{13}C$ of benthic foraminifera *C. wuellerstorfi*, and (b, c) εNd of mixed planktonic foraminifera from cores MD77-169, MD12-3412 (b, this study), MD77-176 (b, Yu et al., 2018; εNd record only), and SK129-CR2 (c, Wilson et al., 2015a) for Terminations I and II. Shaded grey bars represent the Younger Dryas (YD), Henrich Stadial 1 (HS 1), and the Eemian period.

Fig. 7. (a) $\delta^{18}O$ of *C. wuellerstorfi* and (b) εNd values of mixed planktonic foraminifera from cores MD12-3412 (this study) and SK129-CR2 (Wilson et al., 2015a). (c) Past seawater ΔεNd values correlated using AnalySeries software ($\varepsilon Nd_{MD12\text{-}3412}$-$\varepsilon Nd_{SK129}$; black dashed line indicates zero gradient). (d) Indonesian Throughflow (ITF) intensity deduced from thermocline water temperature gradient (ΔTWT; black dashed line serves as a reference at 2 °C) (purple line; Pang et al., 2021) and July insolation at 10°N (yellow line). (e) Global sea-level change (Grant et al., 2014).

Acknowledgments

We thank the two reviewers for their helpful and constructive comments on the original manuscript. DJW was supported by a Natural Environment Research Council independent research fellowship (NE/T011440/1). For the purpose of open access, the author has applied a 'Creative Commons Attribution (CC BY) licence' to any Author Accepted Manuscript version arising. YH acknowledges CSC for supporting her study in France.

References

Abbott, A.N., Haley, B.A., McManus, J., 2015. Bottoms up: Sedimentary control of the deep North Pacific Ocean's εNd signature. *Geology* 43, 1035. https://doi.org/10.1130/G37114.1

Abbott, A.N., Löhr, S.C., Payne, A., Kumar, H., Du, J. 2022. Widespread lithogenic control of marine authigenic neodymium isotope records? Implications for paleoceanographic reconstructions. *Geochim. Cosmochim. Acta* 319, 318-336. https://doi.org/10.1016/j.gca.2021.11.021

Ahmad, S. M., Zheng, H., Raza, W., Zhou, B., Lone, M. A., Raza, T. & Suseela, G., 2012. Glacial to Holocene changes in the surface and deep waters of the northeast Indian Ocean. *Mar. Geol.* 329-331, 16-23. https://doi.org/10.1016/j.margeo.2012.10.002

Ali, S., Hathorne, E. C., Frank, M., Gebregiorgis, D., Stattegger, K., Stumpf, R., Kutterolf, S., Johnson, J. E. & Giosan, L., 2015. South Asian monsoon history over the past 60 kyr recorded by radiogenic isotopes and clay mineral assemblages in the Andaman Sea. *Geochem. Geophys. Geosyst.* 16, 505-521. https://doi.org/10.1002/2014GC005586

Bang, S., Huh, Y., Khim, B.-K., Takata, H., Ikehara, M., Hyeong, K., Seo, I. & Cho, H., 2021. Deep-Water Circulation over the Last Two Glacial Cycles Reconstructed from Authigenic Neodymium Isotopes in the Equatorial Indian Ocean (Core HI1808-GPC04). *Ocean Sci. J.* 57, 324-333. https://doi.org/10.1007/s12601-021-00046-8

Bassinot. F., Beaufort. L., 2012. MD 191 / MONOPOL cruise, RV Marion Dufresne, https://doi.org/10.17600/12200050

Bayon, G., Giresse, P., Chen, H., Rouget, M. L., Gueguen, B., Moizinho, G. R., & Beaufort, D., 2023. The Behavior of Rare Earth Elements during Green Clay Authigenesis on the Congo Continental Shelf. *Minerals*, *13*(8), 1081. https://doi.org/10.3390/min13081081

Bharti, N., Bhushan, R., Skinner,Muruganantham, M., Jena, P. S., Dabhi, A. & Shivam, A., 2022. Evidence of poorly ventilated deep Central Indian Ocean during the last glaciation. *Earth Planet. Sci. Lett.*

582, 117438. https://doi.org/10.1016/j.epsl.2022.117438

Burton, K. W. & Vance, D., 2000. Glacial-interglacial variations in the neodymium isotope composition of seawater in the Bay of Bengal recorded by planktonic foraminifera. *Earth Planet. Sci. Lett.* 425-441. https://doi.org/10.1016/S0012-821X(00)00011-X

Casse, M., Jean-Carlos, M., Guillaume, S., Andre, P., 2019. REE distribution and Nd isotope composition of estuarine waters and bulk sediment leachates tracing lithogenic inputs in eastern Canada. *Mar. Chem.* 211 117–130. https://doi.org/10.1016/j.marchem.2019.03.012

Chamley, H. & Chamley, H., 1989. Clay formation through weathering. *Clay sedimentology*, 21-50. https://doi.org/10.1007/978-3-642-85916-8_2

Chen, J., Farrell, J., Murray, D., and Prell, W., 1995, Timescale and paleoceanographic implications of a 3.6 m.y. oxygen isotope record from the northeast Indian Ocean (Ocean Drilling Program site 758), *Paleoceanogr Paleoclimatol.,* 10, 21– 47. https://doi.org/10.1029/94PA02290.

Colin, C., Turpin, L., Bertaux, J., Desprairies, A. & C.Kissel., 1999. Erosional history of the Himalayan and Burman ranges during the last two glacial–interglacial cycles. *Earth Planet. Sci. Lett.* 171, 647-660. https://doi.org/10.1016/S0012-821X(99)00184-3

Colin, C., Turpin, L., Blamart, D., Frank, N., Kissel, C. & Duchamp, S., 2006. Evolution of weathering patterns in the Indo-Burman Ranges over the last 280 kyr: Effects of sediment provenance on87Sr/86Sr ratios tracer. *Geochem. Geophys. Geosyst.* 7, Q03007. https://doi.org/10.1029/2005GC000962

Copard, K., Colin, C., Douville, E., Freiwald, A., Gudmundsson, G., De Mol, B. & Frank, N., 2010. Nd isotopes in deep-sea corals in the North-eastern Atlantic. *Quat. Sci. Rev.* 29, 2499-2508. https://doi.org/10.1016/j.quascirev.2010.05.025

Curray, J. R., Emmel, F. J. & Moore, D. G., 2003. The Bengal Fan: morphology, geometry, stratigraphy, history and processes. *Mar. Pet. Geol.* 19**,** 1191-1223. https://doi.org/10.1016/S0264-8172(03)00035-7

Damodararao Karri, Singh Sunil K., Rai Vinai K., Ramaswamy V., Rao P. S., 2016. Lithology, Monsoon and Sea-Surface Current Control on Provenance, Dispersal and Deposition of Sediments over the Andaman Continental Shelf. *Front. Mar.*3, 118. https://doi.org/ 10.3389/fmars.2016.00118

Elliot, M., Labeyrie, L. & Duplessy, J.-C., 2002. Changes in North Atlantic deep-water formation associated with the Dansgaard–Oeschger temperature oscillations (60–10ka). *Quat. Sci. Rev.* 21**,** 1153-1165. https://doi.org/10.1016/S0277-3791(01)00137-8

Freeman, E., Skinner, L. C., Tisserand, A., Dokken, T., Timmermann, A., Menviel, L. & Friedrich, T., 2015. An Atlantic–Pacific ventilation seesaw across the last deglaciation. *Earth Planet. Sci. Lett.* 424**,** 237-244. https://doi.org/10.1016/j.epsl.2015.05.032

Galbraith, E. D., Jaccard, S. L., Pedersen, T. F., Sigman, D. M., Haug, G. H., Cook, M., Southon, J. R. & Francois, R., 2007. Carbon dioxide release from the North Pacific abyss during the last deglaciation. *Nature,* 449**,** 890-893. https://doi.org/10.1038/nature06227

Grant, K., Rohling, E., Ramsey, Cheng C. H., Edwards R. L., Florindo F., Heslop D., Marra F., Roberts A. P., Tamisiea M. E.& Williams F., 2014. Sea-level variability over five glacial cycles. *Nat. Commun.* 5, 5076. https://doi.org/10.1038/ncomms6076

Gourlan, A. T., Meynadier, L., Allègre, C. J., Tapponnier, P., Birck, J.-L. & Joron, J.-L., 2010. Northern Hemisphere climate control of the Bengali rivers discharge during the past 4 Ma. *Quat. Sci. Rev.* 29**,** 2484-2498. https://doi.org/10.1016/j.quascirev.2010.05.003

Haley, B.A., Du, J., Abbott, A.N., McManus, J., 2017. The impact of benthic processes on rare earth element and neodymium isotope distributions in the oceans. *Front. Mar. Sci.* 4, 426. https://doi.org/10.3389/fmars.2017.00426

Hindshaw, R. S., Aciego, S. M., Piotrowski, A. M. & Tipper, E. T., 2018. Decoupling of dissolved and bedrock neodymium isotopes during sedimentary cycling. *Geochem. Perspect. Lett.* 8**,** 43-46. doi: 10.7185/geochemlet.1828

Hoogakker, B. A. A., Rohling, E. J., Palmer, M. R., Tyrrell, T. & Rothwell, R. G., 2006. Underlying causes for long-term global ocean δ13C fluctuations over the last 1.20 Myr. *Earth Planet. Sci. Lett.* 248**,** 15-29. https://doi.org/10.1016/j.epsl.2006.05.007

Howe, J. N. W., Piotrowski, A. M. & Rennie, V. C. F., 2016. Abyssal origin for the early Holocene pulse of unradiogenic neodymium isotopes in Atlantic seawater. *Geology,* 44**,** 831-834. https://doi.org/10.1130/G38155.1

Hu, R., Noble, T. L., Piotrowski, A. M., McCave, I. N., Bostock, H. C. & Neil, H. L., 2016. Neodymium isotopic evidence for linked changes in Southeast Atlantic and Southwest Pacific circulation over the last 200 kyr. *Earth Planet. Sci. Lett.* 455**,** 106-114. https://doi.org/10.1016/j.epsl.2016.09.027

Huang, Y., Colin, C., Liu, Z., Douville, E., Dapoigny, A., Haurine, F., Wu, Q. & Tien-Shun Lin, A., 2023. Impacts of nepheloid layers and mineralogical compositions of oceanic margin sediments on REE concentrations and Nd isotopic compositions of seawater. *Geochim. Cosmochim. Acta* 359**,** 57-70. https://doi.org/10.1016/j.gca.2023.08.026

Huyghe, P., Guilbaud, R., Bernet, M., Galy, A. & Gajurel, A. P., 2011. Significance of the clay mineral distribution in fluvial sediments of the Neogene to Recent Himalayan Foreland Basin (west-central Nepal). *Basin Research,* 23**,** 332-345. https://doi.org/10.1111/j.1365-2117.2010.00485.x

Jacobsen, S. B. & Wasserburg, G. J., 1980. Sm-Nd isotopic evolution of chondrites. *Earth Planet. Sci. Lett.* 50**,** 139-155. https://doi.org/10.1016/0012-821X(84)90109-2

Jeandel, C., Thouron, D. & Fieux, M., 1998. Concentrations and isotopic compositions of neodymium in the eastern Indian Ocean and Indonesian straits. *Geochim. Cosmochim. Acta* 62**,** 2597-2607.

https://doi.org/10.1016/S0016-7037(98)00169-0

Joussain, R., Colin, C., Liu, Z., Meynadier, L., Fournier, L., Fauquembergue, K., Zaragosi, S., Schmidt, F., Rojas, V. & Bassinot, F., 2016. Climatic control of sediment transport from the Himalayas to the proximal NE Bengal Fan during the last glacial-interglacial cycle. *Quat. Sci. Rev.* 148**,** 1-16. https://doi.org/10.1016/j.quascirev.2016.06.016

Larkin, C. S., Piotrowski, A. M., Hindshaw, R. S., Bayon, G., Hilton, R. G., Baronas, J. J., Dellinger, M., Wang, R. & Tipper, E. T., 2021. Constraints on the source of reactive phases in sediment from a major Arctic river using neodymium isotopes. *Earth Planet. Sci. Lett.* 565**,** 116933. https://doi.org/10.1016/j.epsl.2021.116933

Lathika, N., Rahaman, W., Tarique, M., Gandhi, N., Kumar, A. & Thamban, M., 2021. Deep water circulation in the Arabian Sea during the last glacial cycle: Implications for paleo-redox condition, carbon sink and atmospheric CO2 variability. *Quat. Sci. Rev.* 257. https://doi.org/10.1016/j.quascirev.2021.106853

Le Houedec, S., Tremblin, M., Champion, A., & Samankassou, E., 2024. Modulation of the northward penetration of Antarctica intermediate waters into the eastern equatorial Indian Ocean under glacial and interglacial conditions. Scientific Reports, 14(1), 6673.

Lupker, M., France-Lanord, C., Galy, V., Lavé, J. & Kudrass, H., 2013. Increasing chemical weathering in the Himalayan system since the Last Glacial Maximum. *Earth Planet. Sci. Lett.* 365**,** 243-252. https://doi.org/10.1016/j.epsl.2013.01.038

Ma, R., Sépulcre, S., Bassinot, F., Haurine, F., Tisnérat-Laborde, N. & Colin, C., 2020. North Indian Ocean Circulation Since the Last Deglaciation as Inferred From New Elemental Ratio Records for Benthic ForaminiferaHoeglundina elegans. *Paleoceanogr. Paleoclimatol.* 35**,** e2019PA003801. https://doi.org/10.1029/2019PA003801

Naik, S. S., Basak, C., Goldstein, S. L., Naidu, P. D. & Naik, S. N., 2019. A 16-kyr Record of Ocean Circulation and Monsoon Intensification From the Central Bay of Bengal. *Geochem. Geophys. Geosyst.* 20**,** 872-882. https://doi.org/10.1029/2018GC007860

Nisha, K., Naik, S. S., Kumar, P., Banerjee, B. & Murty, P. B. R., 2023. Radiocarbon evidence for reduced deep water ventilation of the northern Indian Ocean during the last glacial maxima and early deglaciation. *Earth Planet. Sci. Lett.* 607**,** 118067. https://doi.org/10.1016/j.epsl.2023.118067

Pang, X., Bassinot, F., & Sepulcre, S., 2021. Indonesian Throughflow variability over the last two glacial-interglacial cycles: Evidence from the eastern Indian Ocean. *Quat. Sci. Rev. 256*, 106839. https://doi.org/10.1016/j.quascirev.2021.106839

Piotrowski, A. M., Banakar, V. K., Scrivner, A. E., Elderfield, H., Galy, A. & Dennis, A., 2009. Indian Ocean circulation and productivity during the last glacial cycle. *Earth Planet. Sci. Lett.* 285**,** 179-189. https://doi.org/10.1016/j.epsl.2009.06.007

Piotrowski, A. M., Goldstein, S. L., Sidney, R. H., Fairbanks, R. G., & Zylberberg, D. R., 2008. Oscillating glacial northern and southern deep water formation from combined neodymium and carbon isotopes. *Earth Planet. Sci. Lett. 272*(1-2), 394-405. https://doi.org/10.1016/j.epsl.2008.05.011

Raymo, M. E. & Ruddiman, W. F., 1992. Tectonic forcing of late Cenozoic climate. *Nature,* 359**,** 117-122. https://doi.org/10.1038/359117a0

Sarin, M., Krishnaswami, S., Dilli, K., Somayajulu, B. & Moore, W., 1989. Major ion chemistry of the Ganga-Brahmaputra river system: weathering processes and fluxes to the Bay of Bengal. *Geochim. Cosmochim. Acta* 53**,** 997-1009. https://doi.org/10.1016/0016-7037(89)90205-6

Shankar, D., P. Vinayachandran, and A. Unnikrishnan, 2002. The monsoon currents in the north Indian Ocean, *Prog. Oceanogr.,* 52(1), 63–120. https://doi.org/10.1016/S0079-6611(02)00024-1

Singh, S. K. & France-Lanord, C., 2002. Tracing the distribution of erosion in the Brahmaputra watershed from isotopic compositions of stream sediments. *Earth Planet. Sci. Lett.* 202**,** 645-662. https://doi.org/10.1016/S0012-821X(02)00822-1

Singh, S. P., Singh, S. K., Goswami, V., Bhushan, R. & Rai, V. K., 2012. Spatial distribution of dissolved neodymium and εNd in the Bay of Bengal: Role of particulate matter and mixing of water masses. *Geochim. Cosmochim. Acta* 94**,** 38-56. https://doi.org/10.1016/j.gca.2012.07.017

Song, Z., Wan, S., Colin, C., France-Lanord, C., Yu, Z., Dapoigny, A., Jin, H., Li, M., Zhang, J. & Zhao, D., 2023. Enhanced weathering input from South Asia to the Indian Ocean since the late Eocene. *Sci. Bull*. 68,305-313. https://doi.org/10.1016/j.scib.2023.01.015

Song, Z., Wan, S., Colin, C., Yu, Z., Révillon, S., Jin, H., Zhang, J., Zhao, D., Shi, X. & Li, A., 2021. Paleoenvironmental evolution of South Asia and its link to Himalayan uplift and climatic change since the late Eocene. *Global Planet. Change* 200, 103459. https://doi.org/10.1016/j.gloplacha.2021.103459

Stoll, H. M., Vance, D. & Arevalos, A., 2007. Records of the Nd isotope composition of seawater from the Bay of Bengal: Implications for the impact of Northern Hemisphere cooling on ITCZ movement. *Earth Planet. Sci. Lett.* 255**,** 213-228. https://doi.org/10.1016/j.epsl.2006.12.016

Struve, T., Wilson, D., van de Flierdt, T., Pratt, N., Crocket, K., 2019. Middle Holocene expansion of Pacific Deep Water into the Southern Ocean. *Proc. Natl. Acad. Sci. U.S.A. 117*, 889-894. https://doi.org/10.1073/pnas.1908138117

Tachikawa, K., Piotrowski, A. M. & Bayon, G., 2014. Neodymium associated with foraminiferal carbonate as a recorder of seawater isotopic signatures. *Quat. Sci. Rev.* 88**,** 1-13. https://doi.org/10.1016/j.quascirev.2013.12.027

Tachikawa, K., Toyofuku, T., Basile-Doelsch, I. & Delhaye, T., 2013. Microscale neodymium distribution in sedimentary planktonic foraminiferal tests and associated mineral phases. *Geochim. Cosmochim.*

Acta 100, 11-23. https://doi.org/10.1016/j.gca.2012.10.010

Tanaka, T., Togashi, S., Kamioka, H., Amakawa, H., Kagami, H., Hamamoto, T., Yuhara, M., Orihashi, Y., Yoneda, S., Shimizu, H., Kunimaru, T., Takahashi, K., Yanagi, T., Nakano, T., Fujimaki, H., Shinjo, R., Asahara, Y., Tanimizu, M. & Dragusanu, C., 2000. JNdi-1: a neodymium isotopic reference in consistency with LaJolla neodymium. *Chem. Geol.* 168, 279-281. https://doi.org/10.1016/S0009-2541(00)00198-4

Varkey, M., V. Murty, and A. Suryanarayana, 1996. Physical oceanography of the Bay of Bengal and Andaman Sea, *Oceanogr. Mar. Biol.*, 34, 1–70

von Blanckenburg, F. & Nägler, T. F., 2001. Weathering versus circulation-controlled changes in radiogenic isotope tracer composition of the Labrador Sea and North Atlantic Deep Water. *Paleoceanography,* 16, 424-434. https://doi.org/10.1029/2000PA000550

Wang, P., Tian, J., Cheng, X., Liu, C. & Xu, J., 2004. Major Pleistocene stages in a carbon perspective: The South China Sea record and its global comparison. *Paleoceanography* 19. https://doi.org/10.1029/2003PA000991

Wang, R., Williams, T. J., Hillenbrand, C.-D., Ehrmann, W., Larkin, C. S., Hutchings, A. M. & Piotrowski, A. M., 2022. Boundary processes and neodymium cycling along the Pacific margin of West Antarctica. *Geochim. Cosmochim. Acta* 327, 1-20. https://doi.org/10.1016/j.gca.2022.04.012

Wang, Y., Larsen, T., Lauterbach, S., Andersen, N., Blanz, T., Krebs-Kanzow, U., Gierz, P., Schneider, R., 2022. Higher sea surface temperature in the Indian Ocean during the Last Interglacial weakened the South Asian monsoon. *Proc. Natl. Acad. Sci. U.S.A.* 119, e2107720119 https://doi.org/10.1073/pnas.2107720119

West, A. J., Galy, A. & Bickle, M., 2005. Tectonic and climatic controls on silicate weathering. *Earth Planet. Sci. Lett.* 235, 211-228. https://doi.org/10.1016/j.epsl.2005.03.020

Wilson, D. J., Piotrowski, A. M., Galy, A. & Banakar, V. K., 2015a. Interhemispheric controls on deep ocean circulation and carbon chemistry during the last two glacial cycles. *Paleoceanography,* 30**,** 621-641. https://doi.org/10.1002/2014PA002707

Wilson, D.J., Galy, A., Piotrowski, A.M., Banakar, V.K., 2015b. Quaternary climate modulation of Pb isotopes in the deep Indian Ocean linked to the Himalayan chemical weathering. *Earth Planet. Sci. Lett.* 424, 256-268. https://doi.org/10.1016/j.epsl.2015.05.014

Wu, Q., Colin, C., Liu, Z., Thil, F., Dubois-Dauphin, Q., Frank, N., Tachikawa, K., Bordier, L. & Douville, E., 2015. Neodymium isotopic composition in foraminifera and authigenic phases of the South China Sea sediments: Implications for the hydrology of the North Pacific Ocean over the past 25 kyr. *Geochem. Geophys. Geosyst.* 16**,** 3883-3904. https://doi.org/10.1002/2015GC005871

Yu, Z., Colin, C., Bassinot, F., Wan, S. & Bayon, G, 2020. Climate-Driven Weathering Shifts Between Highlands and Floodplains. *Geochem. Geophys. Geosyst.* 21**,** e2020GC008936. https://doi.org/10.1029/2020GC008936

Yu, Z., Colin, C., Douville, E., Meynadier, L., Duchamp-Alphonse, S., Sepulcre, S., Wan, S., Song, L., Wu, Q., Xu, Z. & Bassinot, F., 2017a. Yttrium and rare earth element partitioning in seawaters from the Bay of Bengal. *Geochem. Geophys. Geosyst.* 18**,** 1388-1403. https://doi.org/10.1002/2016GC006749

Yu, Z., Colin, C., Ma, R., Meynadier, L., Wan, S., Wu, Q., Kallel, N., Sepulcre, S., Dapoigny, A. & Bassinot, F., 2018. Antarctic Intermediate Water penetration into the Northern Indian Ocean during the last deglaciation. *Earth Planet. Sci. Lett.* 500**,** 67-75. https://doi.org/10.1016/j.epsl.2018.08.006

Yu, Z., Colin, C., Meynadier, L., Douville, E., Dapoigny, A., Reverdin, G., Wu, Q., Wan, S., Song, L., Xu, Z. & Bassinot, F., 2017b. Seasonal variations in dissolved neodymium isotope composition in the Bay of Bengal. *Earth Planet. Sci. Lett.* 479**,** 310-321. https://doi.org/10.1016/j.epsl.2017.09.022

Yu, Z., Colin, C., Wilson, D. J., Bayon, G., Song, Z., Sepulcre, S., Dapoigny, A., Li, Y. & Wan, S., 2022. Millennial Variability in Intermediate Ocean Circulation and Indian Monsoonal Weathering Inputs During the Last Deglaciation and Holocene. *Geophys. Res. Lett.* 49**,** e2022GL100003. https://doi.org/10.1029/2022GL100003

Zhao, N., Oppo, D. W., Huang, K. F., Howe, J. N. W., Blusztajn, J. & Keigwin, L. D., 2019. Glacial-interglacial Nd isotope variability of North Atlantic Deep Water modulated by North American ice sheet. *Nat. Commun.* 10**,** 5773. https://doi.org/10.1038/s41467-019-13707-z

Zweng, M. M., 2013. World Ocean Atlas 2013, volume 2: Salinity, edited by S. Levitus and A. Mishonov, in NOAA Atlas NESDIS, 74, 39. http://doi.org/10.7289/V5251G4D

Zorzi C, Goni M F S, Anupama, K, Prasad, S., Hanquiez, V., Johnson, J., Giosan, L.,2015 Indian monsoon variations during three constrasting climate periods: The Holocene, Heinrich Stadial 2 and the last interglacial-glacial transitions. *Quat. Sci. Rev.* 125: 50-60. https://doi.org/10.1016/j.quascirev.2015.06.009

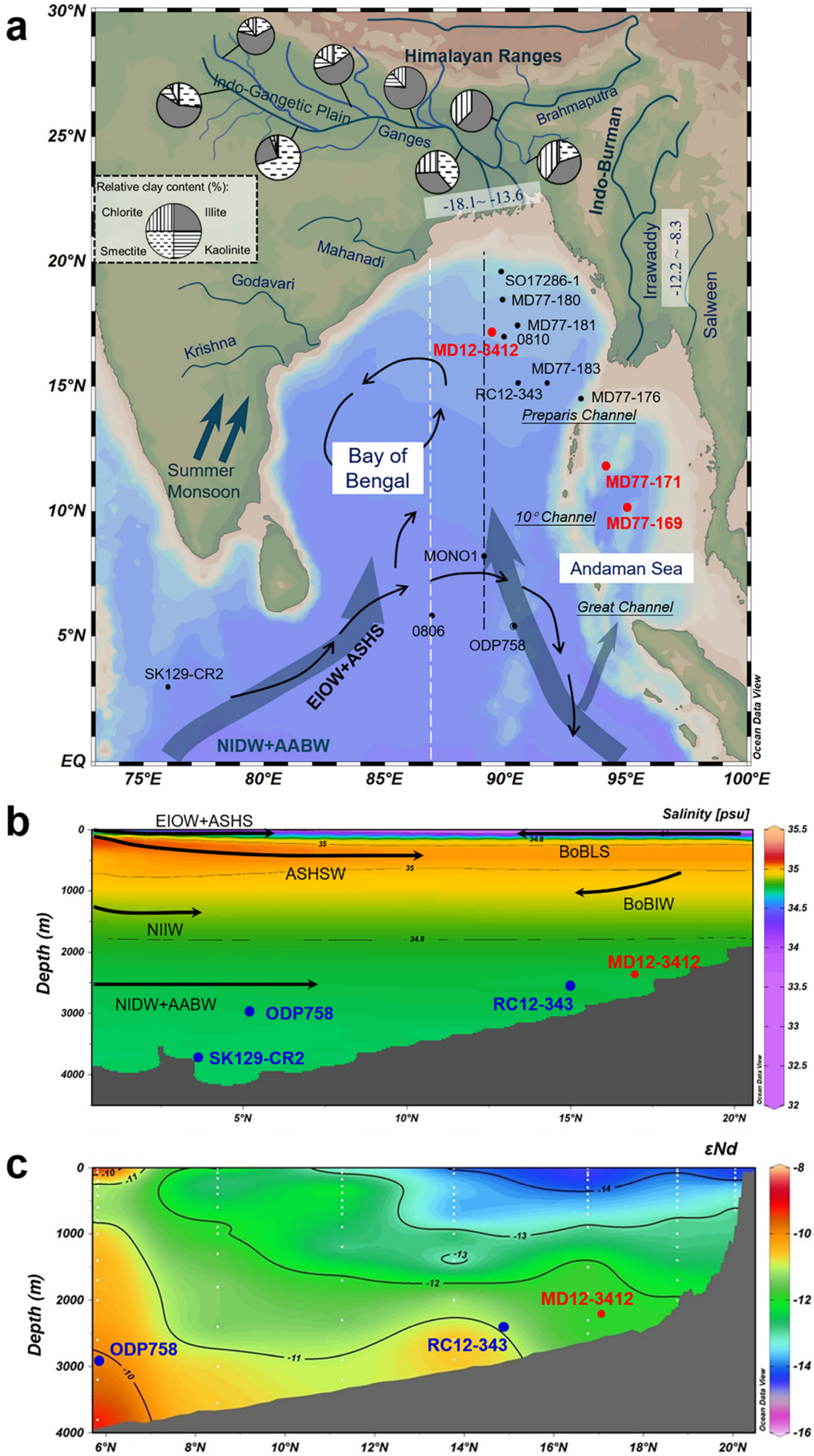

a
Himalayan Ranges
Indo-Gangetic Plain
Ganges
Brahmaputra
Indo-Burman
Irrawaddy
Salween
Mahanadi
Godavari
Krishna
Relative clay content (%):
Chlorite
Illite
Smectite
Kaolinite
-18.1~-13.6
-12.2~-8.3
SO17286-1
MD77-180
MD77-181
0810
MD12-3412
MD77-183
RC12-343
MD77-176
Preparis Channel
Bay of Bengal
Summer Monsoon
MD77-171
MD77-169
10° Channel
MONO1
Andaman Sea
Great Channel
0806
ODP758
EIOW+ASHS
SK129-CR2
NIDW+AABW
Ocean Data View
b
EIOW+ASHS
Salinity [psu]
BoBLS
ASHSW
BoBIW
NIIW
Depth (m)
MD12-3412
NIDW+AABW
ODP758
RC12-343
SK129-CR2
c
εNd
MD12-3412
RC12-343
ODP758
Depth (m)

Fig. 1

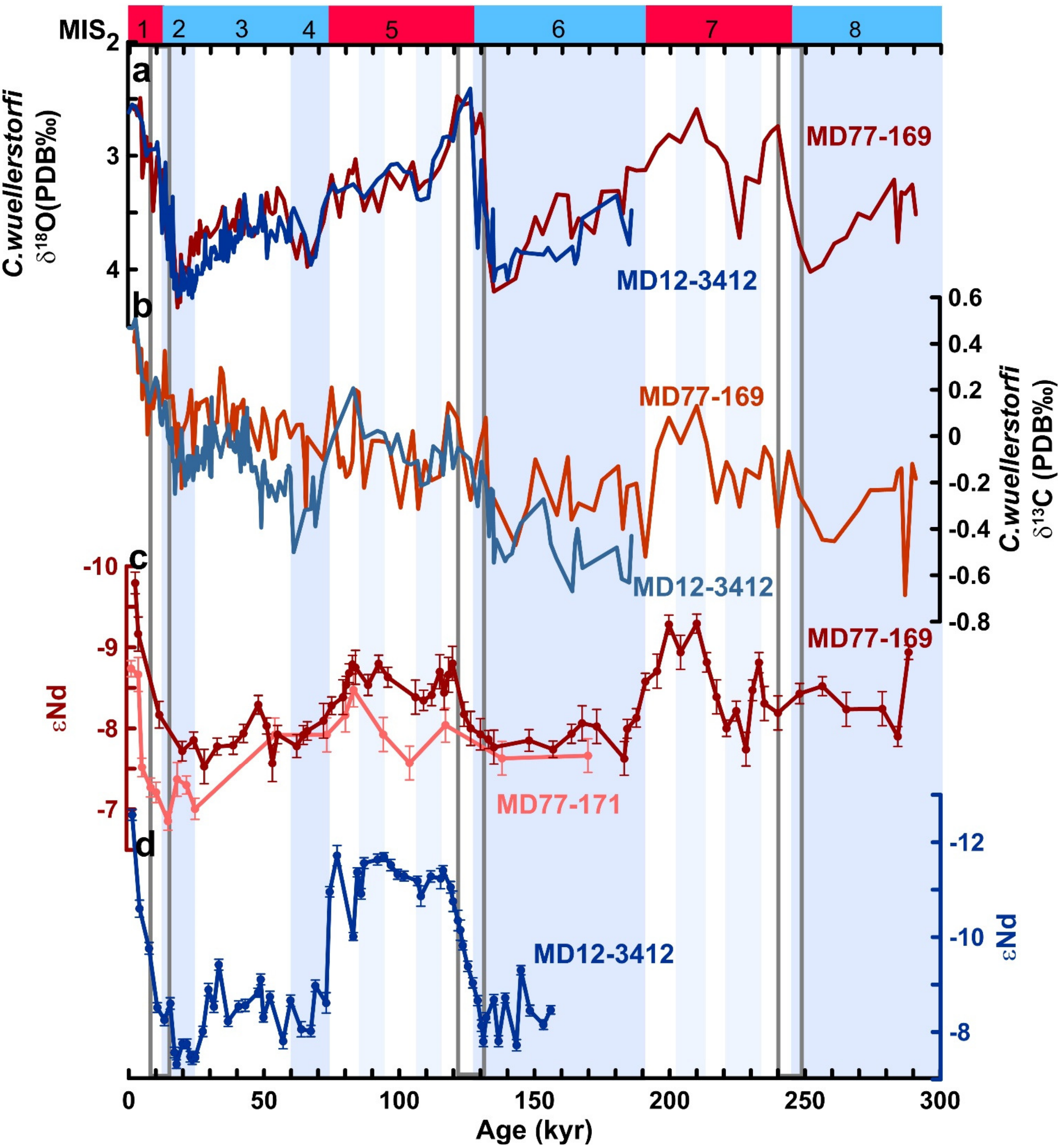
MIS
1
2
3
4
5
6
7
8
a
b
c
d
C.wuellerstorfi δ18O(PDB‰)
C.wuellerstorfi δ13C (PDB‰)
εNd
MD77-169
MD12-3412
MD77-171
Age (kyr)
0
50
100
150
200
250
300

Fig. 2

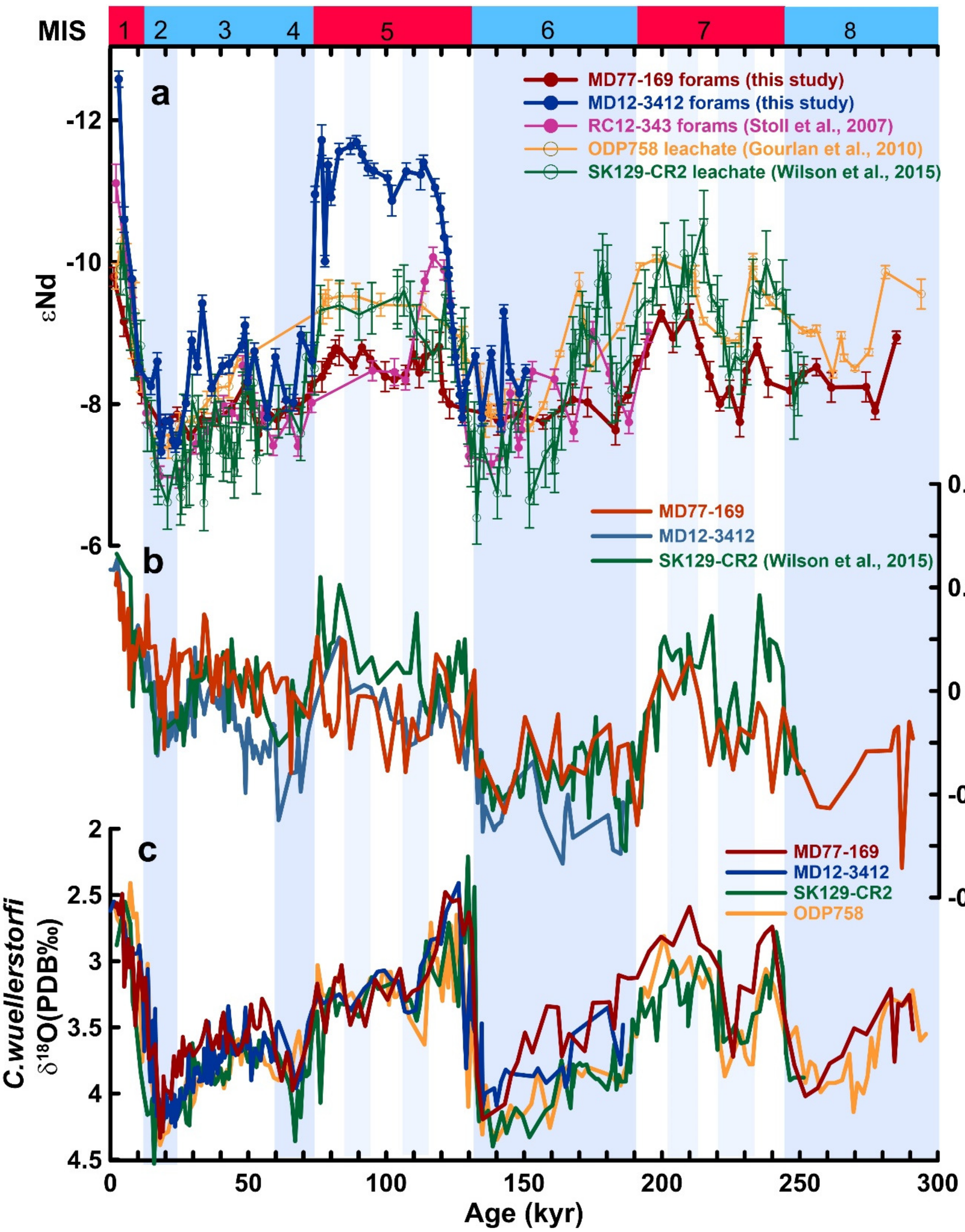
MIS
1
2
3
4
5
6
7
8
a
MD77-169 forams (this study)
MD12-3412 forams (this study)
RC12-343 forams (Stoll et al., 2007)
ODP758 leachate (Gourlan et al., 2010)
SK129-CR2 leachate (Wilson et al., 2015)
εNd
-12
-10
-8
-6
b
MD77-169
MD12-3412
SK129-CR2 (Wilson et al., 2015)
C.wuellerstorfi
δ13C (PDB‰)
0.8
0.4
0
-0.4
-0.8
c
MD77-169
MD12-3412
SK129-CR2
ODP758
C.wuellerstorfi
δ18O(PDB‰)
2
2.5
3
3.5
4
4.5
0
50
100
150
200
250
300
Age (kyr)

Fig.3

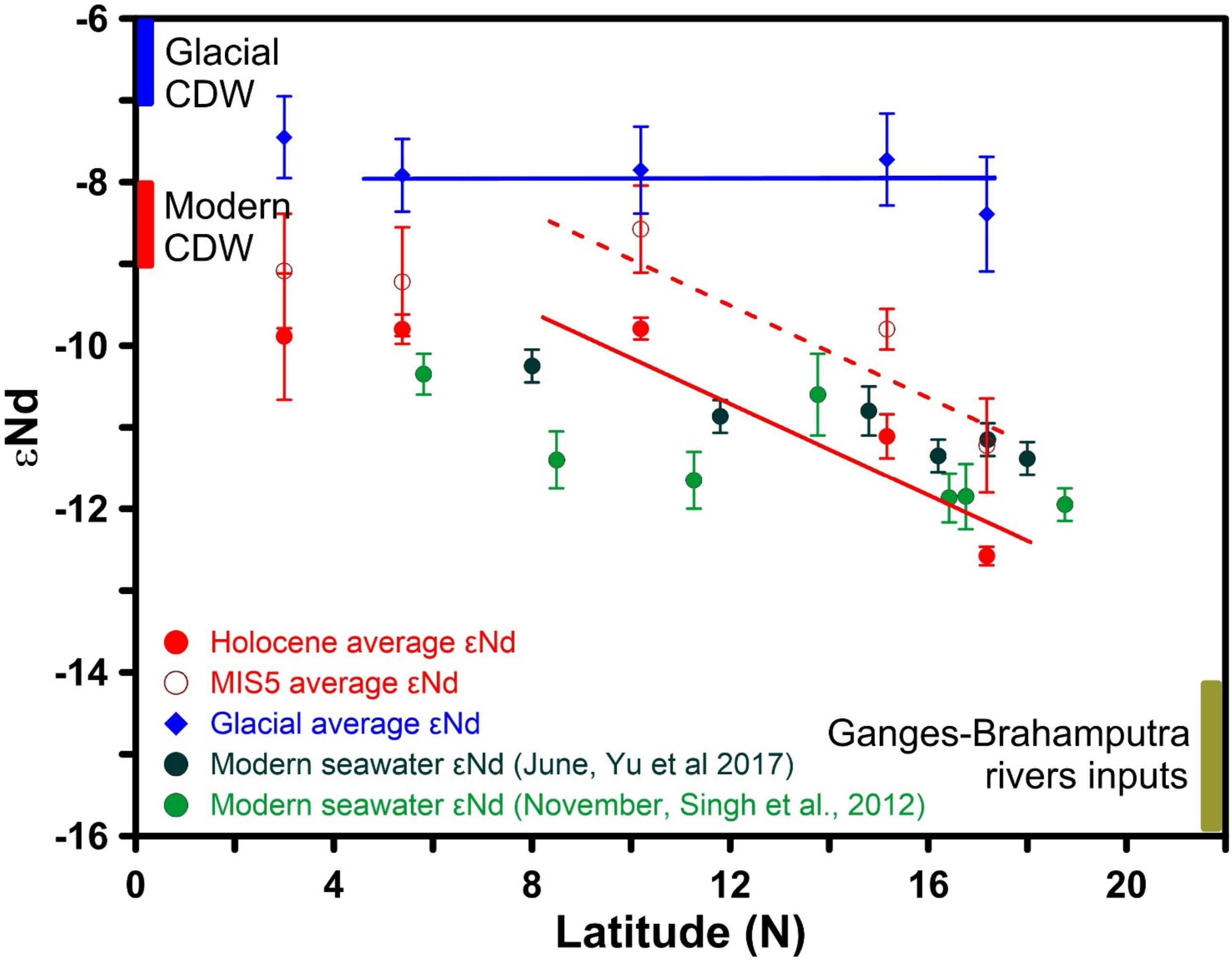

Glacial CDW
Modern CDW
Holocene average εNd
MIS5 average εNd
Glacial average εNd
Modern seawater εNd (June, Yu et al 2017)
Modern seawater εNd (November, Singh et al., 2012)
Ganges-Brahamputra rivers inputs
εNd
Latitude (N)
-6
-8
-10
-12
-14
-16
0
4
8
12
16
20

Fig. 4

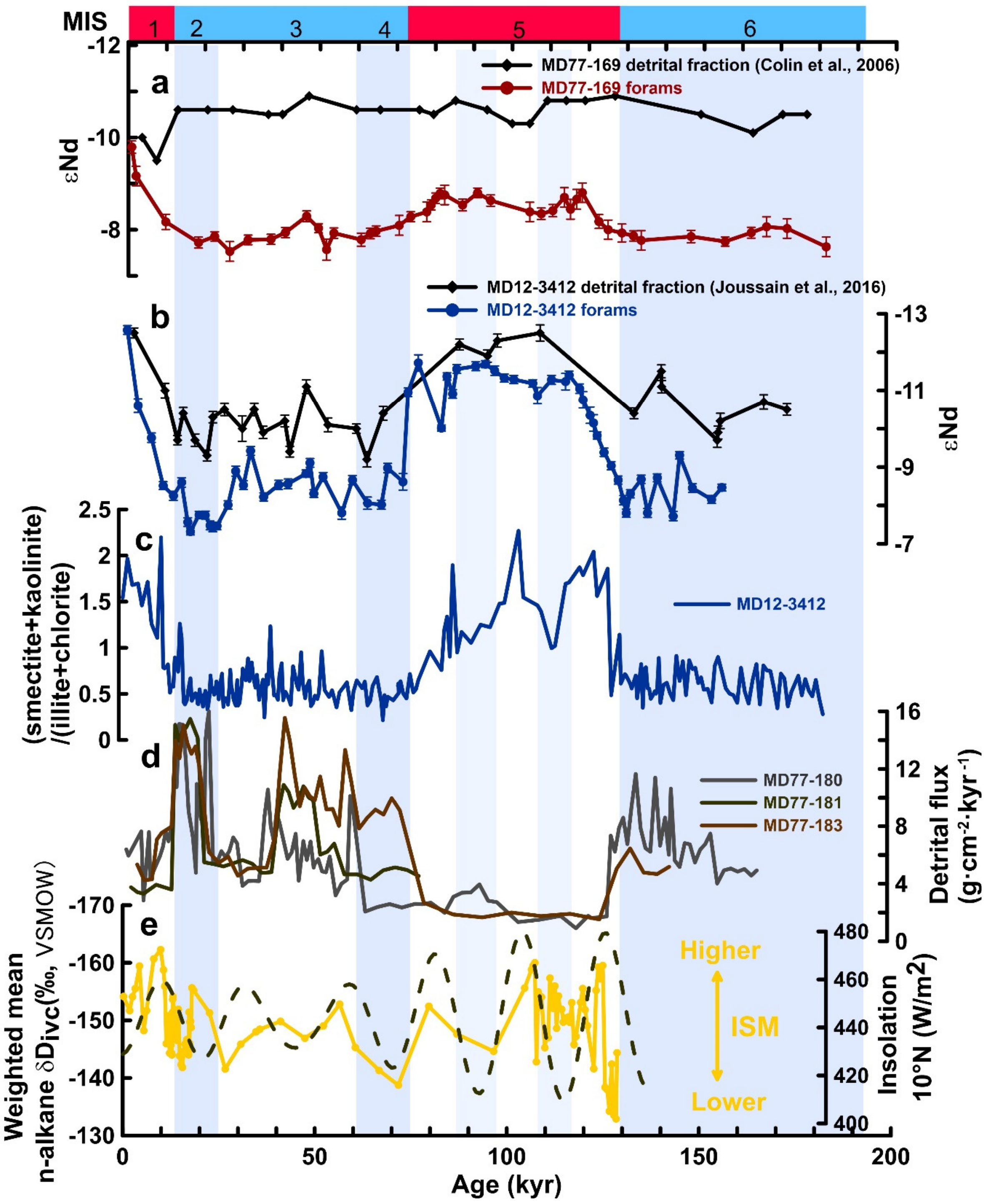
MIS
1
2
3
4
5
6
a
MD77-169 detrital fraction (Colin et al., 2006)
MD77-169 forams
εNd
b
MD12-3412 detrital fraction (Joussain et al., 2016)
MD12-3412 forams
εNd
c
(smectite+kaolinite)
/(illite+chlorite)
MD12-3412
d
MD77-180
MD77-181
MD77-183
Detrital flux
(g·cm⁻²·kyr⁻¹)
e
Weighted mean
n-alkane δDivc(‰, VSMOW)
Higher
ISM
Lower
Insolation
10°N (W/m²)
Age (kyr)

Fig. 5

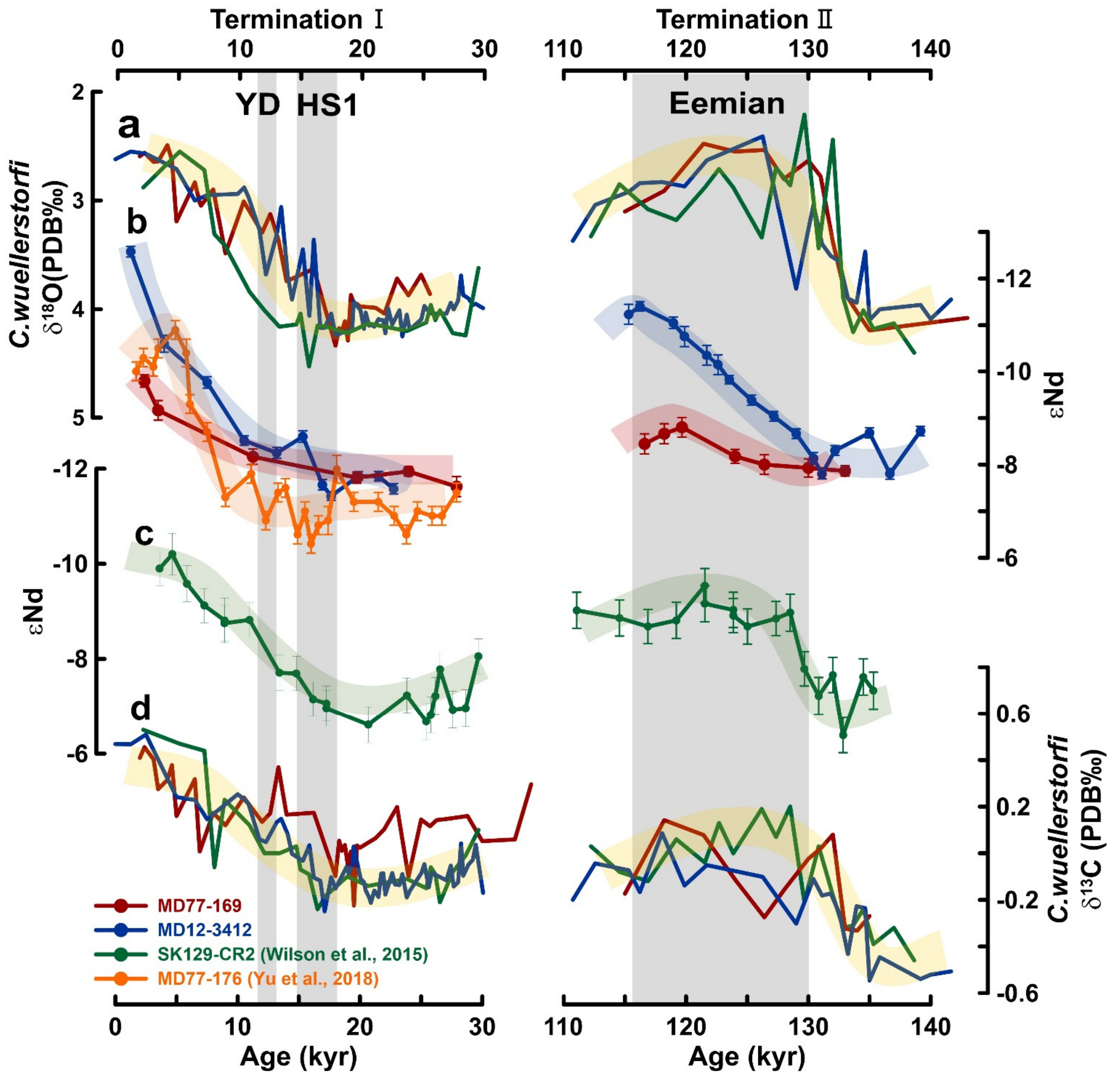
Termination Ⅰ
Termination Ⅱ
YD
HS1
Eemian
a
b
c
d
C.wuellerstorfi δ18O(PDB‰)
εNd
C.wuellerstorfi δ13C (PDB‰)
MD77-169
MD12-3412
SK129-CR2 (Wilson et al., 2015)
MD77-176 (Yu et al., 2018)
Age (kyr)

Fig.6

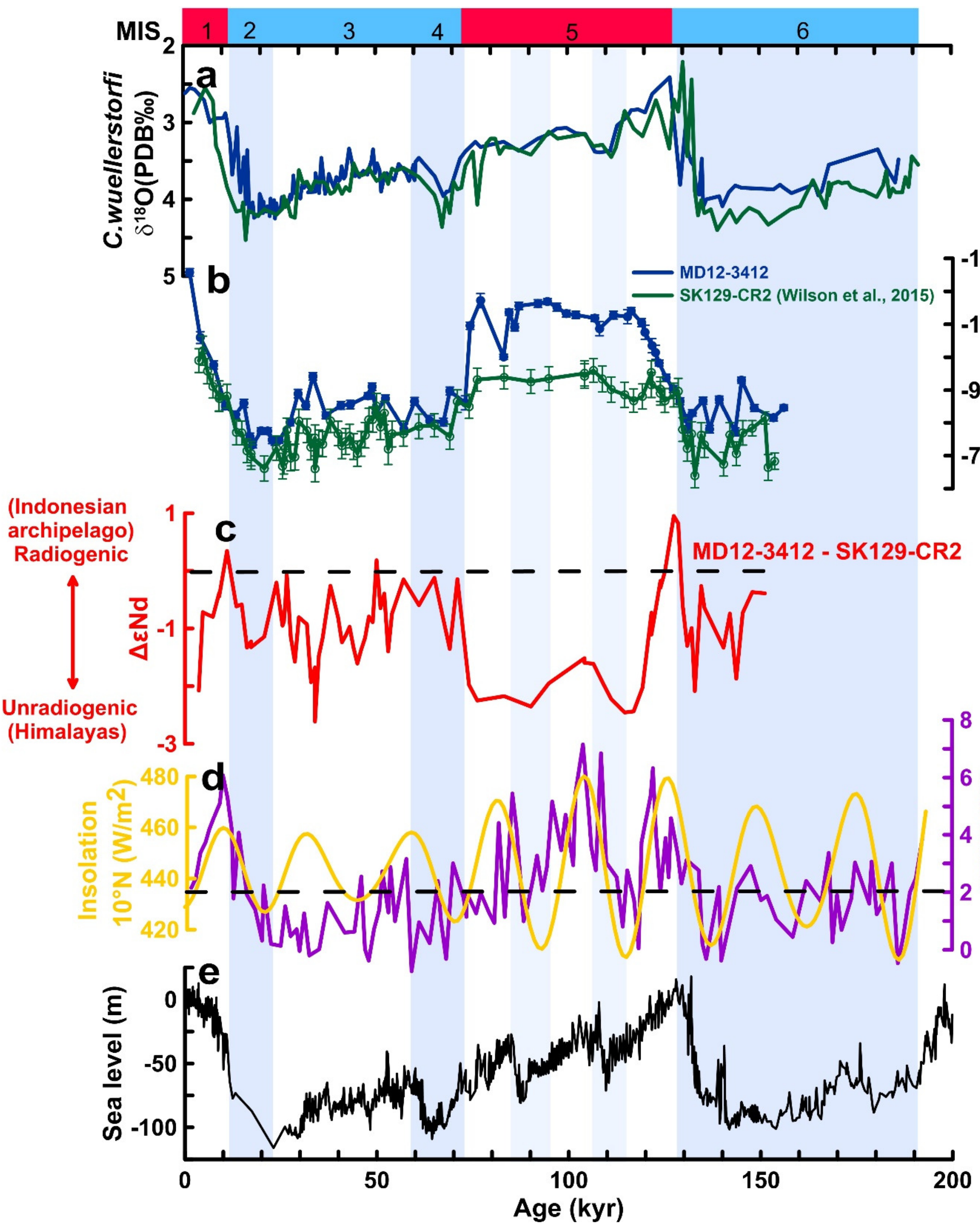

MIS
1
2
3
4
5
6
a
C.wuellerstorfi
δ18O(PDB‰)
b
MD12-3412
SK129-CR2 (Wilson et al., 2015)
εNd
c
(Indonesian archipelago) Radiogenic
Unradiogenic (Himalayas)
ΔεNd
MD12-3412 - SK129-CR2
d
Insolation 10°N (W/m2)
ΔTWT (°C)
Strong
ITF
Weak
e
Sea level (m)
Age (kyr)

Fig. 7

Supplementary information for

Impact of riverine sediment mineralogy on seawater Nd isotope compositions in the northeastern part of the Indian Ocean during the last two glacial cycles

Yi Huang[1, 2], Christophe Colin[2*], Franck Bassinot[3], Zhaojie Yu[4], Quentin Dubois-Dauphin[2], Arnaud Dapoigny[3], David J. Wilson[5], Germain Bayon[6]

1. School of Geosciences and Info-physics, Central South University, 410083, Changsha, China.

2. Université Paris-Saclay, CNRS, GEOPS, 91405, Orsay, France.

3. Laboratoire des Sciences du Climat et de l'Environnement, LSCE/IPSL, CEA, CNRS-UVSQ, Université Paris-Saclay, F-91191 Gif-sur-Yvette, France.

4. Key Laboratory of Marine Geology and Environment, Institute of Oceanology, Chinese Academy of Science, Qingdao, China.

5. Institute of Earth and Planetary Sciences, University College London and Birkbeck, University of London, Gower Street, London, WC1E 6BT, UK.

6. Univ Brest, CNRS, Ifremer, Geo-Ocean, F-29280 Plouzané, France.

**Corresponding author: Christophe Colin – christophe.colin@universite-paris-saclay.fr*

This supplementary information includes:

- Regional setting
- Figure S1, S2

- Table S1, S2

Regional setting

The surface water above 100 m in the Bay of Bengal (BoB) mainly results from the mixing of Eastern Indian Ocean surface water (EIOW) and Arabian Sea High Salinity Water (ASHSW) from the southern BoB and Low Salinity water from the northern BoB (BoBLS) (Fig. 1b). The low salinity of the BoBLS is a result of enhanced freshwater discharge from the Ganges-Brahmaputra (G-B) river system during the summer monsoon period (Talley et al., 2011). The present-day surface currents display seasonal reversals in direction and intensity driven by the changes in the wind pattern associated with the Indian monsoon. Specifically, during the summer months, the surface circulation in the BoB is clockwise, while in winter it is anti-clockwise (Chauhan and Voselgang et al., 2006).

The intermediate waters (500-1500 m) are mainly composed of BoB Intermediate Water (BoBIW) in the northern BoB and high-salinity North Indian Intermediate Water (NIIW) in the southern BoB, which is transported from the Arabian Sea mainly during the Indian summer monsoon period (Wyrtki 1973, Singh et al., 2012) (Fig. 1b). Antarctic Intermediate Water (AAIW) is found at 1000-1500 m depth in the southern Indian Ocean and has been observed almost as far north as 10°S in the modern day (Tomczak and Godfrey 2003).

At greater water depths (from 1200 to 3800 m), a component of North Atlantic Deep Water (NADW) is advected from the Atlantic sector of the Southern Ocean and partially mixes with overlying and underlying water masses during its northwards transit in the Indian Ocean to form North Indian Deep Water (NIDW) (You 2000, Wyrtki 1973) (Fig. 1b). The abyssal depths deeper than 3800 m are occupied by cold Antarctic Bottom Water (AABW) formed in the Weddell Sea (Naveira Garabato et al., 2002) and Ross Sea (Kolla et al., 1976). The AABW also upwells and mixes with NIDW during its northward flow (Fig. 1b), and contributes significantly to the deep-water masses of the BoB.

The Andaman Sea is a semi-enclosed basin connected to the BoB by the Preparis Channel (sill depth of 250 m), the Ten Degree Channel (sill depth of 800 m), and the Great Channel (sill depth of 1800 m) (Fig. 1a). Consequently, the shallow depth of sills between the BoB and the Andaman Sea limits hydrological exchange between these basins to intermediate water masses. The deep water of the Andaman Sea mainly derives from the southern Indian Ocean through the Great Channel (Fig. 1a) (Gayathri et al., 2022).

The G-B river system is characterized by one of the highest sediment discharges (~1x10^9 t/yr) and physical denudation rates (~760 to 930 mm/km^2/yr) in the world (Milliman and Farnsworth, 2011), representing ~12% of the total sediment discharge to the global ocean (Milliman and Farnsworth, 2011). The εNd values of G-B river sediments vary from -18.1 to -13.6 (Singh and France-Lanord, 2002; Singh et al., 2008). The Irrawaddy River, which originates in the Indo-Burman Ranges and the eastern margins of the Himalayan range, is the third largest river in this region, with a sediment discharge of ~325×10^6 t/yr. The εNd values of its river sediments range from -12.2 to -8.3 (Colin et al., 1999, Allen et al., 2008, Damodararao et al., 2016). In comparison, the east Indian rivers and the Arakan coastal rivers are more modest sedimentary sources to the BoB, with lower total sediment discharges of 236×10^6 t/yr and 130×10^6 t/yr, respectively (Milliman and Farnsworth, 2011).

In total, 95% of the annual G-B River and Irrawaddy River sediments are transferred to the BoB and the Andaman Sea during the wet summer monsoon season (Singh et al., 2007). Due to the large freshwater influx during the wet summer monsoon, a plume of reduced sea surface salinity (~7‰) can be observed spreading southwards as far as 15°N in the BoB (Levitus et al., 1994). Sediment and freshwater discharges from these large river basins are thus very reactive to the monsoon rainfall and display a seasonal distribution at the surface of the BoB (Yu et al., 2017b). The BoB is therefore a key region to assess the effects of lithogenic input on seawater εNd values because it receives radiogenic water masses from the Southern Ocean (εNd ~ -8) in its southern part, and large inputs of unradiogenic sediments (εNd ~ -14 to -16) from erosion of the Himalayas via the G-B river systems in its northern part.

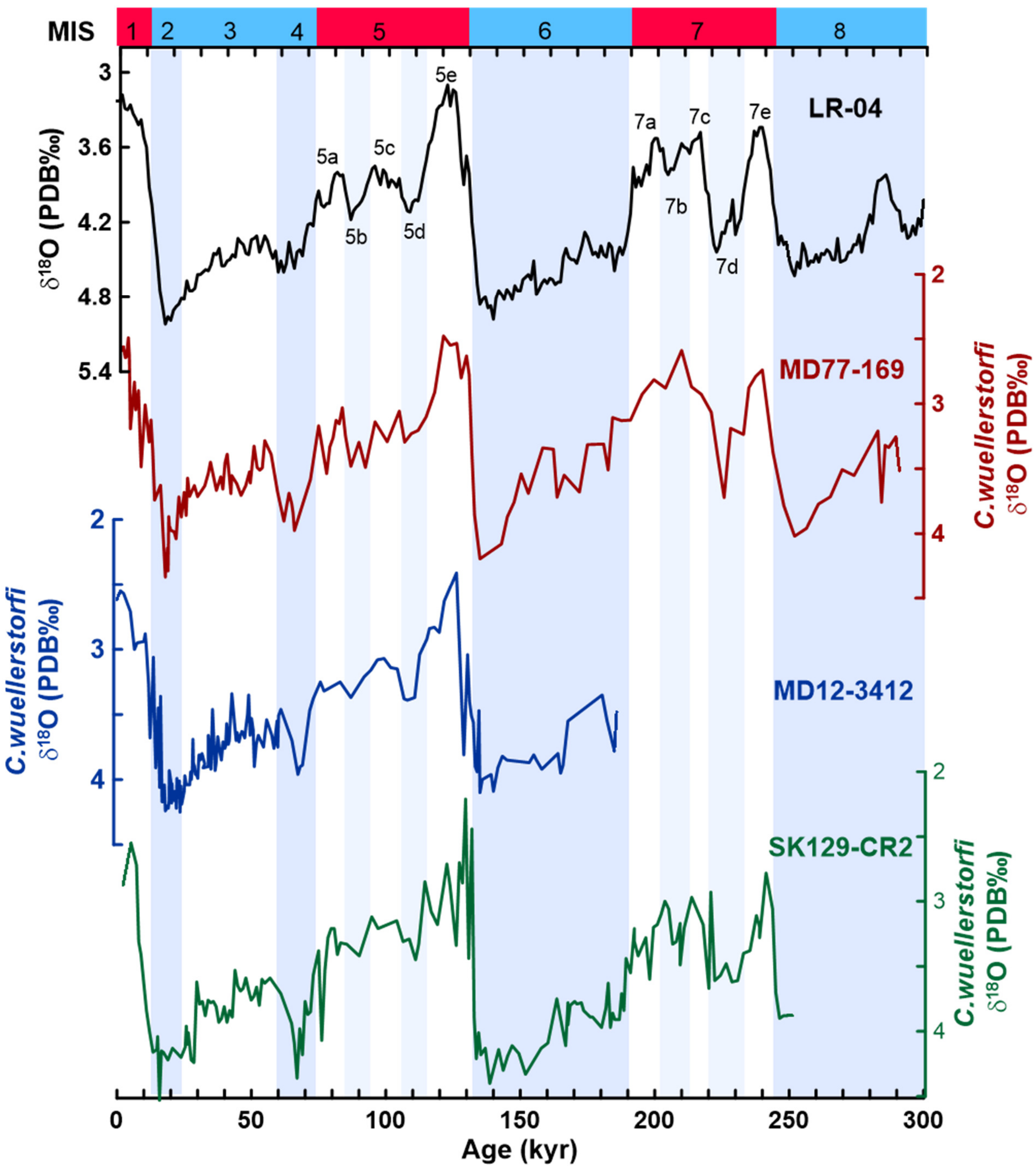

Fig. S1. Age models of cores MD77-169, MD12-3412 (this study), and SK129-CR2 (Wilson et al., 2015). (a) LR-04 stack $\delta^{18}O$ record (Lisiecki and Raymo, 2005), with warm and cold sub-stages of MIS 5 and MIS 7 labelled; (b, c, d) $\delta^{18}O$ of benthic foraminifera *C. wuellerstorfi* in cores MD77-169 and MD12-3412 are tuned to the LR-04 record using *AnalySeries software* (Paillard et al., 1996).

Supplementary References:

Allen, R., Carter, A., Najman, Y., Bandopadhyay, P. C., Chapman, H. J., Bickle, M. J., Garzanti, E., Vezzoli, G., Andò, S., Foster, G. L. & Gerring, C. 2008. New constraints on the sedimentation and uplift history of the Andaman-Nicobar accretionary prism, South Andaman Island. In *Formation and Applications of the Sedimentary Record in Arc Collision Zones,* Geological Society of America. https://doi.org/10.1130/2008.2436(11)

Colin, C., Turpin, L., Bertaux, J., Desprairies, A. & C.Kissel., 1999. Erosional history of the Himalayan and Burman ranges during the last two glacial–interglacial cycles. *Earth Planet. Sci. Lett.* 171**,** 647-660. https://doi.org/10.1016/S0012-821X(99)00184-3

Chauhan, O.S., Vogelsang, E, 2006. Climate induced changes in the circulation and dispersal patterns of the fluvial sources during late Quaternary in the middle Bengal Fan. *J Earth Syst Sci,* **115**, 379–386. https://doi.org/10.1007/BF02702050

Gayathri, N. M., Sijinkumar, A. V., Nath, B. N., Sandeep, K. & Wei, K. Y., 2022. A ~30 kyr sub-centennial to millennial Indian summer monsoon variability record from the southern Andaman Sea, northeastern Indian Ocean. *Palaeogeogr. Palaeoclimatol. Palaeoecol.* 590, 110865. https://doi.org/10.1016/j.palaeo.2022.110865

Damodararao Karri, Singh Sunil K., Rai Vinai K., Ramaswamy V., Rao P. S., 2016. Lithology, monsoon and sea-surface current control on provenance, dispersal and deposition of sediments over the Andaman continental shelf. *Front. Mar. Sci*. 3, 118. https://doi.org/10.3389/fmars.2016.00118

Kolla, V., Moore, D. G. & Curray, J. R., 1976. Recent bottom-current activity in the deep western Bay of Bengal. *Mar. Geol.,* 21**,** 255-270. https://doi.org/10.1016/0025-3227(76)90010-4

Levitus, S., Burgett, R. & Boyer, T. P., 1994. World Ocean Atlas 1994. Vol. 3, Salinity.

Lisiecki, L.E., Raymo, M.E., 2005. A Pliocene-Pleistocene stack of 57 globally distributed benthic d^{18}O records.

Paleoceanography 20, PA1003. https://doi.org/10.1029/2004PA001071

Milliman J D, Farnsworth K L. River discharge to the coastal ocean: a global synthesis[M]. Cambridge University Press, 2011.

Naveira Garabato, A. C., McDonagh, E. L., Stevens, D. P., Heywood, K. J. & Sanders, R. J., 2002. On the export of Antarctic Bottom Water from the Weddell Sea. *Deep Sea Res. Part II: Topical Studies in Oceanography,* 49**,** 4715-4742. https://doi.org/10.1016/S0967-0645(02)00156-X

Singh, S. K. & France-Lanord, C., 2002. Tracing the distribution of erosion in the Brahmaputra watershed from isotopic compositions of stream sediments. *Earth Planet. Sci. Lett.* 202**,** 645-662. https://doi.org/10.1016/S0012-821X(02)00822-1

Singh, S. K., Rai, S. K., Krishnaswami. S., 2008. Sr and Nd isotopes in river sediments from the Ganga Basin: Sediment provenance and spatial variability in physical erosion. *J. Geophys. Res.* 113, F03006. https://doi.org/10.1029/2007JF000909

Singh, S. P., Singh, S. K., Goswami, V., Bhushan, R. & Rai, V. K., 2012. Spatial distribution of dissolved neodymium and εNd in the Bay of Bengal: Role of particulate matter and mixing of water masses. *Geochim. Cosmochim. Acta,* 94**,** 38-56.

Talley, L. D., Pickard, G. L., Emery, W. J., & Swift, J. H., 2011.. Preface. In descriptive physical oceanography (sixth edition), (pp. 1–383). Boston: Academic Press.

Tomczak, M. & Godfrey, J. S. 2003. Hydrology of the Indian Ocean. In *Regional Oceanography,* eds. M. Tomczak & J. S. Godfrey. Amsterdam: Pergamon.

Varkey, M., V. Murty, and A. Suryanarayana, 1996. Physical oceanography of the Bay of Bengal and Andaman Sea, *Oceanogr. Mar. Biol.*, 34, 1–70.

Wyrtki, K. 1973. Physical Oceanography of the Indian Ocean. In *The Biology of the Indian Ocean,* eds. B. Zeitzschel

& S. A. Gerlach, 18-36. Berlin, Heidelberg: Springer Berlin Heidelberg.

You, Y., 2000. Implications of the deep circulation and ventilation of the Indian Ocean on the renewal mechanism of North Atlantic Deep Water. *J. Geophys. Res.: Oceans,* 105**,** 23895-23926. https://doi.org/10.1029/2000JC900105

Yu, Z., Colin, C., Ma, R., Meynadier, L., Wan, S., Wu, Q., Kallel, N., Sepulcre, S., Dapoigny, A. & Bassinot, F., 2018. Antarctic Intermediate Water penetration into the Northern Indian Ocean during the last deglaciation. *Earth Planet. Sci. Lett.* 500**,** 67-75. https://doi.org/10.1016/j.epsl.2018.08.006